Modulation of Lightning Occurrence by the Solar Wind

THESIS

Adam L Baxter, Captain, USAF

AFIT-ENP-MS-20-M-079

DEPARTMENT OF THE AIR FORCE
AIR UNIVERSITY

AIR FORCE INSTITUTE OF TECHNOLOGY

Wright-Patterson Air Force Base, Ohio

AFIT-ENP-MS-20-M-079

Modulation of Lightning Occurrence by the Solar Wind

THESIS

Presented to the Faculty

Department of Engineering Physics

Graduate School of Engineering and Management

Air Force Institute of Technology

Air University

Air Education and Training Command

in Partial Fulfillment of the Requirements for the

Degree of Master of Science in Applied Physics

Adam L Baxter, B.S. Physics

Captain, USAF

March 26, 2020

AFIT-ENP-MS-20-M-079

Modulation of Lightning Occurrence by the Solar Wind

THESIS

Adam L Baxter, B.S. Physics
Captain, USAF

Committee Membership:

Lt Col Anthony L Franz, Ph.D
Chair

Maj Omar A Nava, Ph.D
Member

Maj Daniel J Emmons, Ph.D
Member

Abstract

The influence of solar wind events on the frequency of lightning occurrence has not been studied on a global scale, thereby limiting weather forecasting that includes solar wind and terrestrial weather. Lightning affects military and civilian operations by impacting areas such as communications, power grids, radar, and mission execution. Multiple networks exist that record lightning strikes across the globe using different processing techniques. An understanding of the differences in the networks will allow for more robust weather prediction models. Characterization of the distribution of global lightning strikes based on solar wind events will make progress toward a seamless space-terrestrial environment model. This study presents an analysis of lightning strikes by latitude using a median analysis of event windows during which a solar wind event occurred. Karhunen-Loeve Decomposition (KLD) was also used to find patterns in the distribution of lightning by latitude and a median analysis of the KLD representation of the data was done. The median analysis by latitude gave different results for the Vaisala and Earth Network datasets. The KLD pulled out some common features such as the seasonal dependence and a general increase in lightning at the equator. Comparisons between different datasets must be handled carefully. The KLD method may be a way to capture common features, or assess how similar the datasets are. A detailed analysis of the differences between the two networks detection algorithms and investigating other space weather parameters should be accomplished in the future.

Table of Contents

List of Figures

I. Introduction

Lightning impacts on military operations range from examples such as mission execution, radar interference, and communication disruptions. The connection between terrestrial and space weather phenomena is an emerging field of study [1, 2, 3, 4] with implications for different aspects of operational weather forecasting. It is necessary to understand where and when lightning will occur so that military and civilian operations can continue without disruption. It is desirable to understand any correlation between space environment observables and lightning occurrence. One of the many space environment observables that is recorded by satellites is the speed of the solar wind [5, 6]. It is postulated that the speed of the solar wind modulates galactic cosmic ray (GCR) flux which may be the trigger for lightning initiation [1, 7]. GCR flux is not analyzed in this study.

It is speculated that a sensitivity to geomagnetic latitude exists because of the orientation of Earth's magnetic field lines relative to the surface. At higher latitudes, the field lines are more perpendicular, enhancing the transport of energetic particles into the lower atmosphere that may facilitate lightning onset. In contrast, because magnetic field lines near the equator are oriented more parallel relative to Earth's surface, lightning occurrence should be less sensitive to solar wind events.

The objective of this study is to investigate and characterize the influence of solar wind velocity events on the frequency of lightning occurrence based on latitude. Global lightning strikes will be analyzed by three methods. First, following the methodology similar of Scott et al [1], lightning observations from Vaisala and

Earth Networks will be analyzed against solar wind velocity events obtained through Omniweb using data from the Advanced Composition Explorer (ACE) and Deep Space Climate Observatory (DSCOVR) satellites from 2010 to 2018 in a dataset that was provided by Air Force Institute of Technology faculty. The second method is the Karhunen-Loève Decomposition. This method is used because it efficiently represents variation in the data and can capture global patterns of lightning. A third method combines the first two into a KLD event window analysis.

Chapter 2 will give basic background information about the solar wind, lightning, detection networks and contains a summary of the literature reviewed. Chapter 3 describes the methodologies used in this analysis. A description of the data is followed by a description of the median, the Karhunen-Loève Decomposition (KLD) and KLD event window analysis. The results are given in Chapter 4 with a Fast Fourier Transform used as a comparison tool to the KLD. Conclusions are discussed in Chapter 5, followed by possible future work.

II. Background and Literature Review

The solar wind is comprised of solar energetic particles that stream from the sun at speeds between 400 and 2000 km/s [1]. Satellite measurements for this study are from the ACE and DSCOVR satellites located at the L1 Lagrange point as shown in Figure 1 [5, 6, 8]. Source regions connected to the heliospheric magnetic field (HMF) through 'open' field lines are associated with high speed solar wind streams while source regions with 'closed' magnetic topology are associated with slow solar wind streams [1]. As the solar wind pressure increases, the size of the magnetosphere decreases, its plasma density increases, and the excess plasma is pushed along the magnetic field into the ionosphere [3]. The decrease in the solar wind pressure leads to an increase in the magnetosphere volume, which becomes filled with the ionospheric plasma [3]. These changes may, or may not, have a direct effect on terrestrial lightning strikes.

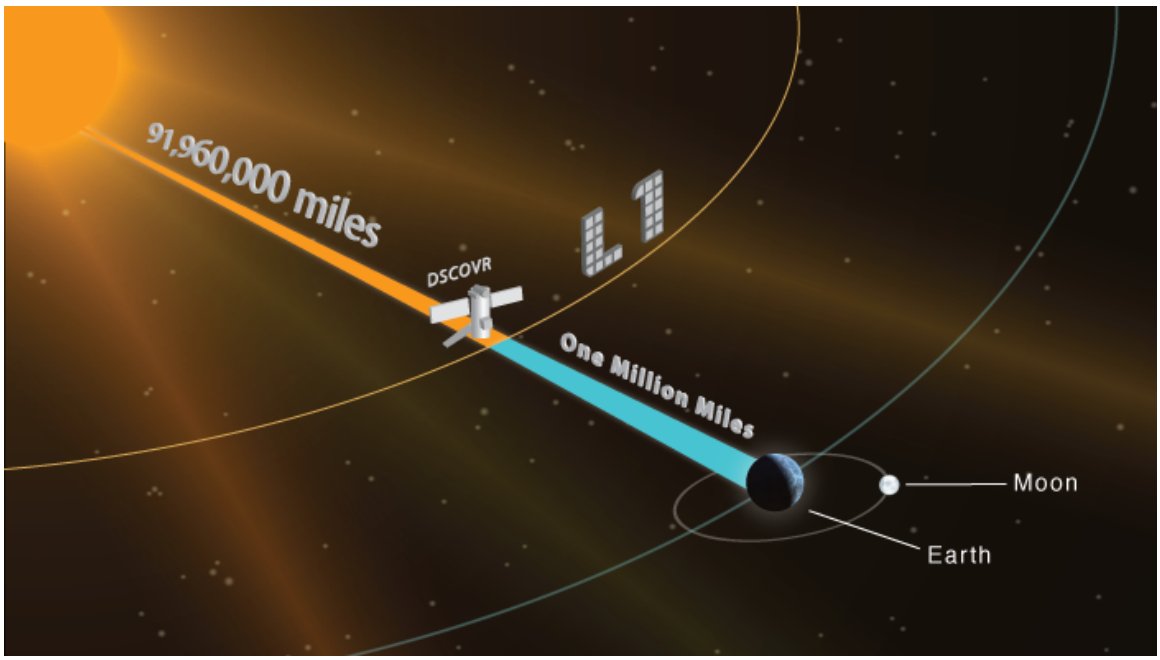

Figure 1: Artist's rendering showing the location of the DSCOVR spacecraft located one million miles between the Earth and the Sun. Credit NASA [8]

Lightning is an electrical discharge created by a charge separation in the atmosphere between clouds, the air, or the ground [9]. The precise trigger of lightning initiation is still not understood and may be caused by solar energetic particles or galactic cosmic rays [1]. The overall frequency range of lightning is reported to be 1 Hz to 300 MHz [10, 11]. An example of the spectrum can be seen in Figure 2 from David M. Le Vine [10]. Lightning produces radio waves called radio atmospherics, or sferics for short, in the Very Low Frequency (VLF) range of 3-30 kHz. The VLF range is used because it contains the highest spectral density of lightning sferics [12]. It is these sferics that are analyzed by various organizations around the world to determine strike characteristics and location. The sferics can travel for thousands of kilometers through the Earth Ionosphere wave guide due to the small amount of attenuation before they are detected by a sensor. Most sensors are located in the northern hemisphere because there is more land to set up sensors. Studies have shown a tendency for stronger, but fewer, flashes over the oceans than over land [13].

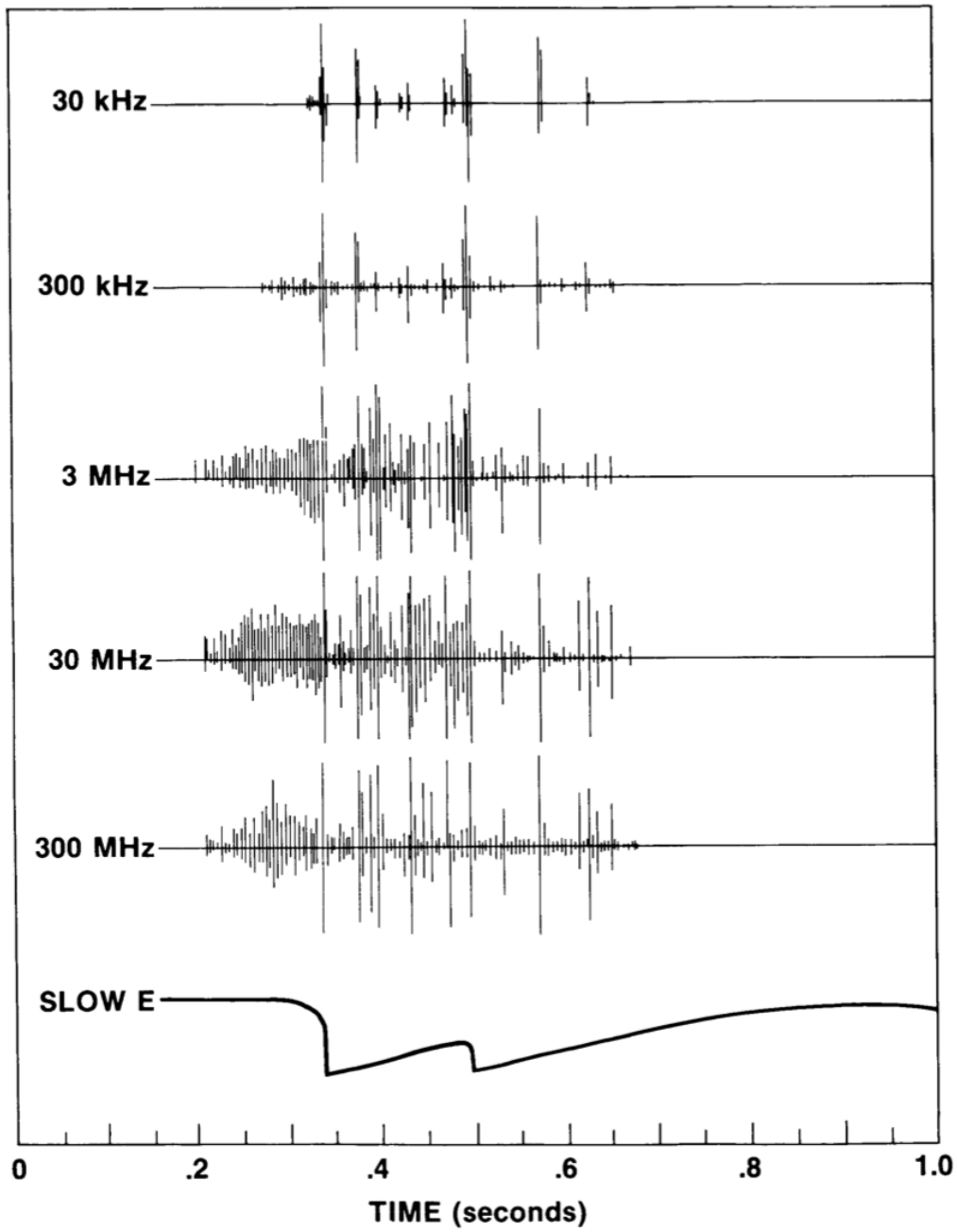

Figure 2: Radiation from a cloud-to-ground lightning flash. The signals at 3-300 MHz are data recorded by the Levine [10]. The examples at 30 and 300 kHz are an estimate based on measurements reported in the literature [10].

2.1 Lightning Detection Networks

One of the global networks that detects lightning is run by the Vaisala company. They have sensors across the globe as well as operate the National Lightning Detection Network (NLDN) in the US [11]. This network measures sferics with frequencies of 400 Hz to 400kHz and uses magnetic direction finding and advanced time-of-arrival to analyze the lightning strike [14, 11]. Rudolsky et al [15] paraphrased a detailed description of the Vaisala Global Lightning Dataset (GLD360) methodology by Said et al [16, 17] with the following:

> The waveform matching algorithm begins by cross correlating the measured sferic with a locally stored waveform bank. The waveform bank is composed of sferic waveforms from negative [cloud to ground] CG strokes indexed at distances ranging from 100 to 6000 km. There is a separate waveform bank for daytime and nighttime propagation conditions. Each detected sferic is cross correlated with the appropriate waveform bank using both the sferic and its negative (i.e., inverse). The peak cross correlation of each polarity determines an estimated distance for that polarity. Once an initial location fix is determined at the central processor, the true propagation distance to each sensor is compared with the estimated propagation distances for each polarity. The polarity that results in the smallest estimated propagation distance error gives the estimated polarity from the respective sensor. The overall polarity for the discharge is determined from a weighted sum of the polarity estimates from each contributing sensor. The resulting dataset provides a record of all lightning discharges observed by at least three GLD360 sensors. [15]

Earth Networks Global Lightning Network (ENGLN) is another lightning detec-

tion network. They have partnered with the University of Washington's World Wide Lightning Location Network (WWLLN) [18]. Most of the sensors are located in the northern hemisphere [19]. The network has sites that record the vertical electric field component from 1 Hz to 12 MHz and the pulses in the electric field are located by time of arrival, and grouped into flashes [20, 21]. The time of group arrival (TOGA) of a sferic is that instant when the regression line of phase versus frequency over a specified band has zero slope [12]. Rodger et al. [22] discussed that a new TOGA algorithm was being developed that would be less sensitive to interference of multiple lightning events occurring at the same time. Multiple events are clustered into a single waveform for analysis if they are within 700 milliseconds and 10 km [23]. The Earth Networks sensors are a wide-band system enabling the sensor to not only detect strong CG strokes, but to also detect weak IC pulses[21]. The sensor records whole waveforms of each flash and sends them back, in compressed data packets, to the central server where the whole waveforms are used in locating the flashes and differentiating between intra-cloud (IC) and CG strokes [21]. At least four sites are needed to determine the location at which the lightning occurred [12].

2.2 Literature Review

Lightning has been observed across the globe. It has been studied by various people over specific areas and countries such as Finland, Saudi Arabia, Brazil and the United Kingdom [24, 25, 2, 1]. It is also studied on other planets [26]. The paper will focus on Earth based studies that discuss lightning and the solar wind.

In 2014 Owens et al [27] accomplished a study on the modulation of lightning over the United Kingdom by the heliospheric magnetic field (HMF) polarity.

> The large-scale HMF consists of sectors of toward (T) and away (A) polarity, which are known to skew the Earth's magnetic field in oppos-

ing manners. In [27], UK lightning and thunder rates are shown to be significantly different when the Earth is embedded in T or A sectors, with 40–60% more thunderstorm activity in T sectors than A sectors. This result persists even when the strong seasonal variation in thunderstorm activity is removed. Comparing with global neutron monitor measurements, this does not seem to be solely the result of changes in the global top-of-the-atmosphere energetic charged particle flux, which is the mechanism by which previous studies have suggested solar modulation of lightning. Instead, we propose a redistribution of lightning, rather than a global change in the lightning rate. The T/A-sector skewing of the Earth's magnetic field relative to a fixed geographic position will change both the local ionospheric potential and the atmospheric footprints of various energetic charged particle populations. This, in turn, may change the discharge processes in electrified storm clouds, though the mechanisms have yet to be established [27].

In a paper by Scott et al [1], it was found by using the arrival of a high-speed stream at Earth defined as an increase of the solar wind v_y component, which points in the direction opposite of Earth's orbit direction, by more than 75 km/s over 5 hrs, that the lightning increased for approximately 40 days over the UK. These trigger events defined by the solar wind speed variation were analyzed by using a composting, or super-posed, method [1]. Scott et al. used the same arrival time difference (ATD) lightning detection system by the UK Met Office for the lightning strike counts as Owens et al did [1].

The thunderstorm activity in relation to solar activities was also studied over the country of Brazil. The solar activity is represented by the International Sunspot Number (ISN) compiled by the National Oceanic and Atmospheric Administration

(NOAA) from the World Data Center for the Sunspot Index, Royal Observatory of Belgium [2]. Seven cities were investigated by using the respective recorded thunder day data [2]. Six out seven cities investigated exhibit periodicities near 11 years [2]. The results suggest a significant correlation between solar and thunderstorm activity, from 1951 to 2009, for three out seven cities with an anti-phase behavior [2]. It is postulated that magnetic shielding effects at low latitude stations may promote anti-phase behavior, but that in-phase behavior may be more prevalent at high latitudes if the energetic radiation from the Sun during solar max are more prevalent then and these particles are less effectively shielded [2].

2.3 Karhunen-Loève Decomposition

The Karhunen-Loève Decomposition (KLD) is recognized under a number of other aliases such as proper orthogonal decomposition, principal component analysis, and empirical orthogonal functions [28]. Early uses of KLD included analysis of turbulent flows, simulations, model reduction, and catalytic reaction-diffusion experiments [29]. In its basic form, the KL decomposition is the detection of spatially coherent modes in dynamics of a spatiotemporally varying system through the diagonalization of the covariance matrix of an ensemble of data [29]. The eigenvectors corresponding to the dominant eigenvalues of this matrix are the "structures" that capture most of the coherence of the data set [29]. In particular, the projection onto the first n-eigenvectors captures more of the "energy" (mean square fluctuation) than any other n-mode projection [29]. In this sense, the KL eigenvectors provide an optimal basis for a vector-valued data set where the ensemble average of the data is subtracted out, so only fluctuations are analyzed [29]. The basis is optimal in the sense that it converges faster on average than any other representation [30].

Another common analysis method is the Fourier Transform (FT). It is not heavily

used in this study but it is applied as a reference point and for certain comparisons to the KLD method. The KLD method is more useful in this analysis compared to a Fourier Transform for the following reasons. First, it is a more flexible transform because the basis functions can be of any form [31]. The basis functions are not restricted to sines and cosines like the Fourier Transform. Second, the data is not required to be periodic [31]. Comparatively the FT is best suited for periodic functions and may not perform well under non-periodic conditions. Third, the KLD coefficients reflect the stochastic nature of the data better than the FT coefficients [31].

III. Methodology

3.1 Data

The solar wind data was provided by the Omniweb website run by NASA. This dataset is in 1 hr increments spanning from 1 Jan 2010 to 31 Dec 2017 as shown in Figure 3. The solar wind speed was used to find a trigger event. The trigger criteria used is defined as an increase in the solar wind speed of 75 km/s or more within 5 hours. This gave a total of 479 days on which a trigger event(s) occurred shown in Figure 3 as red dots. There are no apparent seasonal distribution of solar wind speed spikes. If a single day had multiple trigger events, the additional events were ignored and the day was counted just once. 47 trigger event days were not used in the analysis since the trigger event day would cause the analysis window to extend beyond the start/end of the dataset as the analysis window is $\pm$ 60 days of the trigger event day. The window of $\pm$ 60 days is used so that trends may be seen as well as following the Scott et al. paper [1]. The total speed of the solar wind was used as the data was already in that form and the components of the speed were not available from OmniWeb. Scott et al used the v_y velocity in their analysis [1].

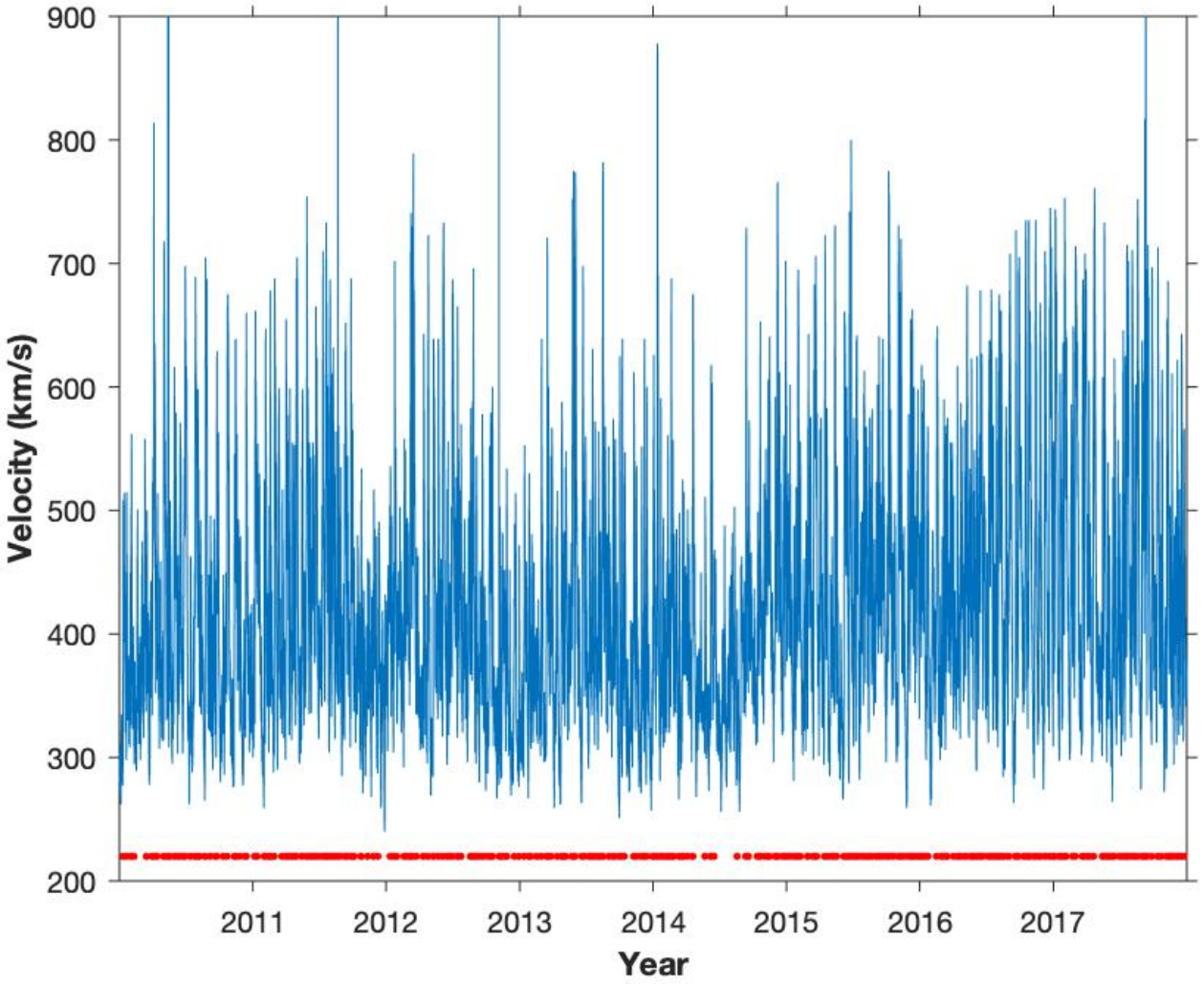

Figure 3: The solar wind velocity over seven years. The four data points that go beyond the bounds of the graph were changed to the previous reasonable speed and therefore were ignored in the analysis. The source of these anomalies was not found during the research for this study.

The entire dataset of lightning strokes was provided by the 14th Weather Squadron, USAF. The source of the dataset being comprised of only the global networks or a combination of US and global sensors is unknown. There was no reply from the 14th Weather Squadron after initial contact. It contains the number of strikes per day, specifying the latitude and longitude where the strike(s) occurred in one degree res-

olution covering the entire globe. The data begins on 1 Jan 2010 and ends 21 Aug 2017 by combining data from two different networks, the Vaisala and Earth Networks as shown in Figures 4 and 5, with an overlapping day on 26 Feb 2013.

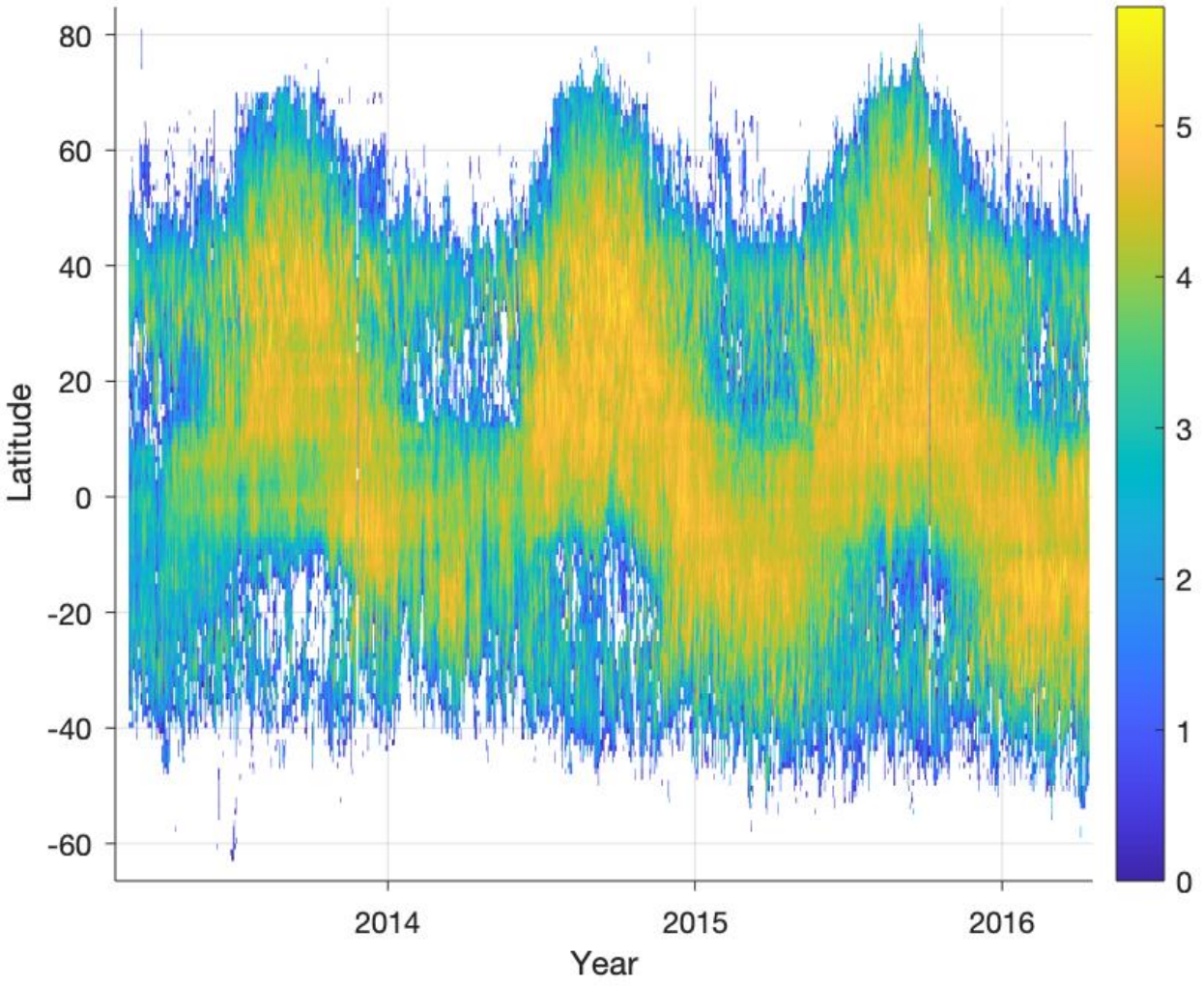

Figure 4: A log plot of the number of strikes per latitude over time of the Vaisala data. Seasonal variations can be seen in the wave pattern with an increase in lightning during the summer months in the northern hemisphere and the winter months in the southern hemisphere. The log was used to so that smaller details were not washed out by large number of strikes due to areas of high lightning concentration. The maximum number of strikes for a single data point from this dataset is 266672.

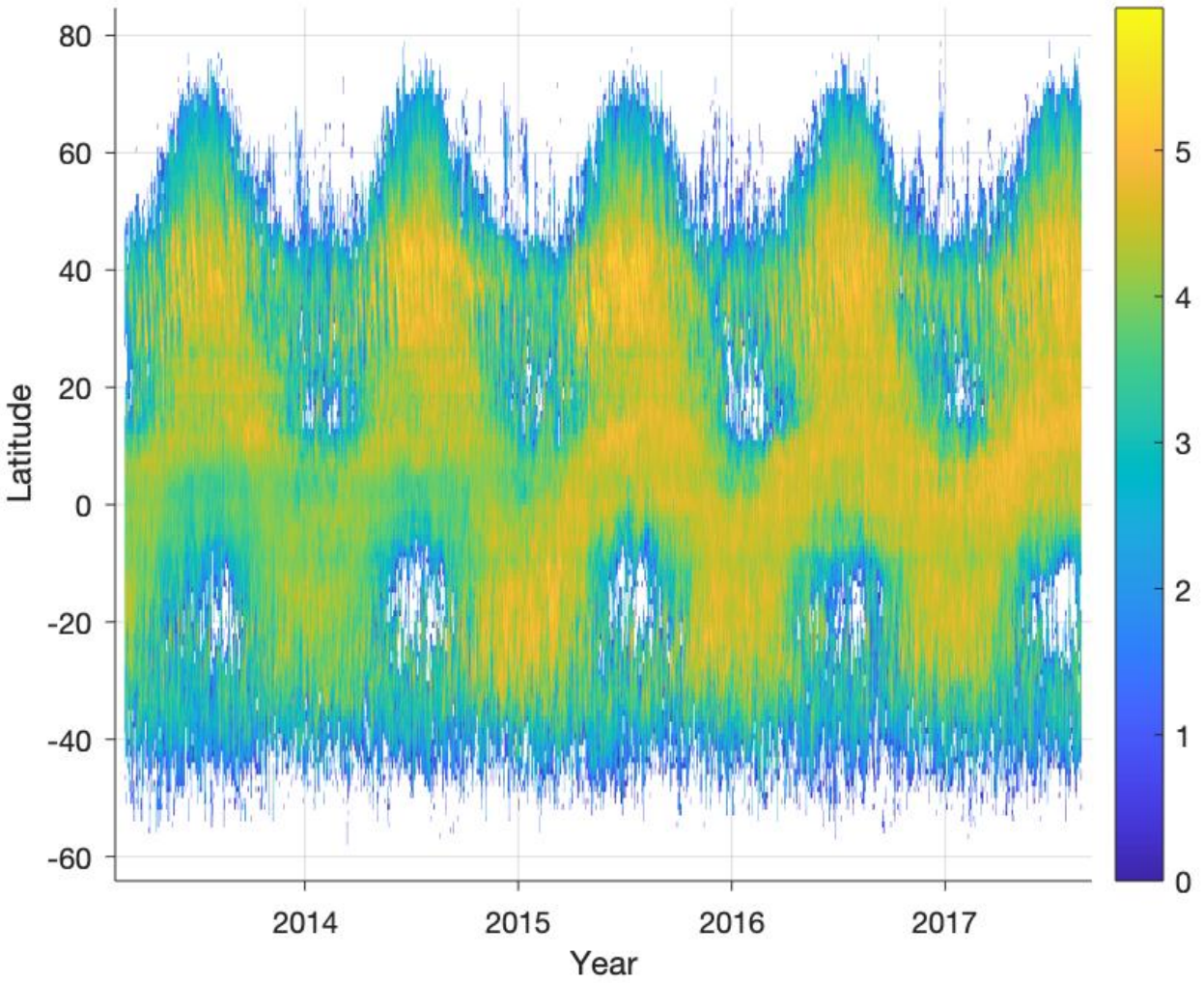

Figure 5: A log plot of the number of strikes per latitude over time of the Earth Network data. Seasonal variations can be seen in the wave pattern with an increase in lightning during the summer months in the northern hemisphere and the winter months in the southern hemisphere. The log was used to so that smaller details were not washed out by large number of strikes due to areas of high lightning concentration. The maximum number of strikes for a single data point from this dataset is 284593.

The duplicate day was found by visually scanning the data for the change from one network to another and verified using MATLAB. The first part of the data, 1 Jan 2010 - 26 Feb 2013, is from the Vaisala Network. The remaining part of the data is from the Earth Network. The duplicate day was found to contain data from both

networks, but not all the data points were the same. Each network had strikes located at different geographical locations. The duplicate day was analyzed and found that the Earth Network data counted 266,971 more strikes than the Vaisala Network for the same latitudes and longitudes, see Figure 6. Since the data overlapped on only one day and the strike counts were vastly different, it was deemed that it should be split into two different sets of data and analyzed separately. These two datasets were further organized by the number of strikes per latitude by day.

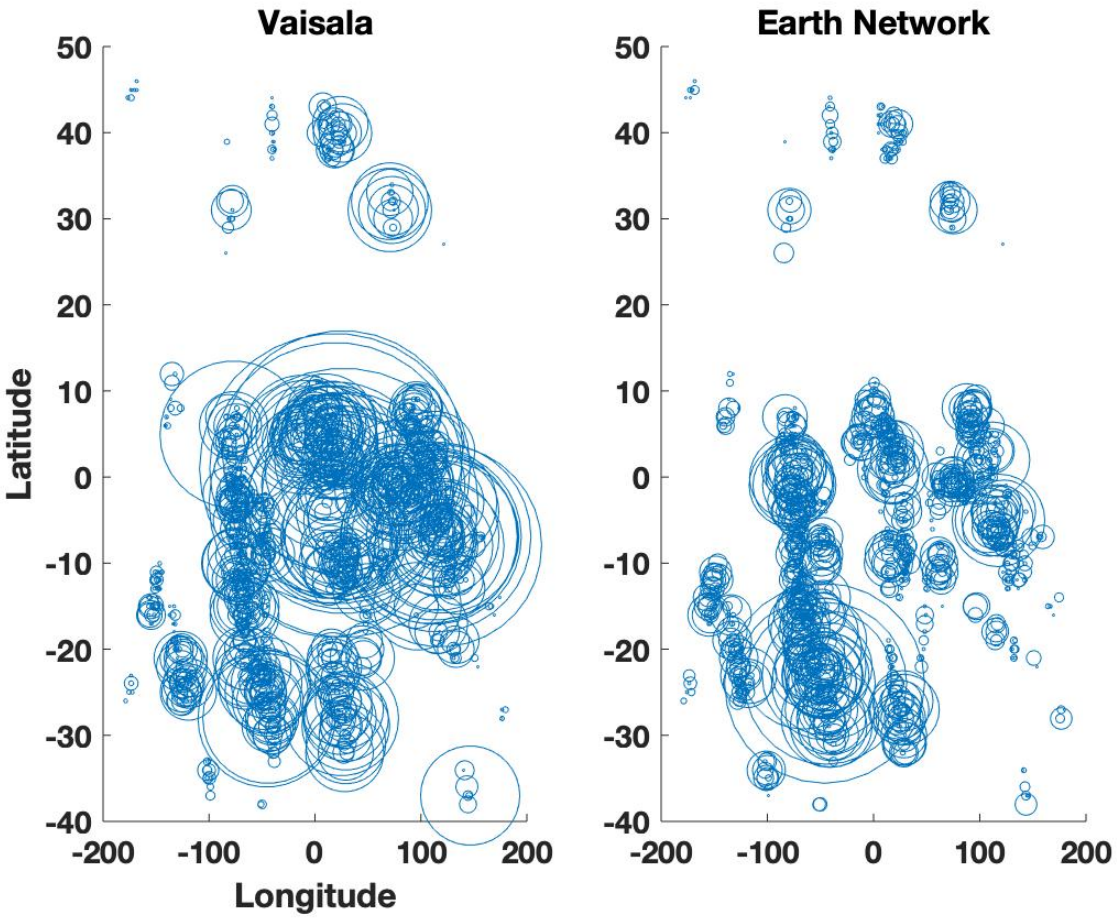

Figure 6: The duplicate day was found to contain 266,971 more strikes in the Earth Network data (b) than the Vaisala data (a). The size of the circles indicate the number of lightning strikes. The Vaisla data shows a high amount of lightning around the Democratic Republic of Congo, a place of known active lightning strikes. The southern hemisphere shows more lightning than the northern because it is winter in the northern hemisphere.

3.2 Median Calculation

The median of the raw number of lightning strikes per latitude by day for all trigger event windows of ±60 days was calculated by following Scott's work in [1]. The median was used instead of the mean so that large outliers in the data would not dominate. This was calculated in MATLAB for both sets of data. If multiple trigger days occur inside an existing event window, the calculation was still made and the lightning is counted as normal.

3.3 Karhunen-Loève Decomposition

The KLD portion of the analysis was also accomplished in MATLAB by adapting code from previous work done by Lt Col Franz [32]. The KLD technique has not been used in lightning strike analysis as of the time of this report. Additional properties of the KLD lend well to this analysis and are introduced below.

KLD is a statistical method for compressing spatiotemporal data by finding the largest linear subspace that contains substantial statistical variation of the data [33]. The modes are orthogonal and are defined by the data constituting a natural coordinate system that approximate the data optimally [34]. The following description of the KLD is based on Triandaf et al [34].

The procedure applies to a discretized spatiotemporal pattern given in terms of a computational spatial grid $\mathbf{x} =(x_1,\ldots,x_p)$, and at discrete intervals in time t_n:

$$\{u^n(x)\} = \{\mathbf{u}(x,t_n)\}_{n=1,M} \tag{1}$$

The KL eigenmodes are the eigenfunctions of the autocorrelation matrix $\mathbf{K}(x,x')$. This matrix is given by

$$\mathbf{K}(x, x') = \langle \mathbf{u}(x, t)\mathbf{u}(x', t) \rangle \tag{2}$$

where the brackets stand for time average and the vector product is the dyadic product. The field $\mathbf{u}$ may be expanded as

$$\mathbf{u}(x, t) = \sum_n \alpha_n(t)\psi_n(x) \tag{3}$$

where $\psi_n(x)$ are the KLD basis modes [34] and $\alpha_n(t)$ are the coefficients that weight the impact of the eigenmodes [32] at each time. The coefficients are calculated by $\alpha_n(t) = \sum_n \mathbf{u}'(x, t)\psi_n(x)$ where the prime indicates a transpose [32]. Eigenvalues are related to the coefficients by

$$\lambda_n = \langle \alpha_n(t)\alpha_n(t) \rangle \tag{4}$$

where the brackets denote a time average [28].

Another useful property is that the KL basis minimizes Shannon's entropy [28, 35], meaning that the entropy, or amount of information, is the smallest that it can be. This is important because is supports the KLD property that the basis modes are optimal for the data [35]. Entropy also gives a single number associated with the complexity of the system or data; higher numbers mean more complex data. The entropy is calculated by $\mathbf{H} = -\sum \lambda_i log(\lambda_i)$, where λ_i are the normalized eigenvalues [28]. Entropy can be calculated from the eigenvalues of a FT using the same equation. The entropy was verified to be lower using KLD vs FT by comparing Earth Network data on which a Fast Fourier Transform (FFT) was performed which gave a value of 4.1 compared to the KLD that gave 2.8. Vaisala gives values of 3.9 and 2.9 for the FFT and KLD expansions respectively. As a reference, a random matrix with the same dimensions as the Vaisala data gave an entropy of 5.1 for the KLD expansion.

The KLD was implemented after the lightning data was organized into a matrix of days (rows) and latitude (columns) by summing all the strikes for a single day per latitude and repeating for all days and latitudes. This allows for the analysis to find any latitudinal dependence that may exist. Once the data is in this form the mean of each latitude is subtracted before it is fed into the KLD code where the autocorrelation matrix $\mathbf{K}$ is calculated using (2) and the eigenvalue problem is solved using MATLAB's *eig* function. This gives 181 eigenmodes and eigenvalues from the 181 latitude values from $\pm 90^{\circ}$ including 0°. The eigenvalues are normalized by the sum of the eigenvalues. These eigenvalues are sorted largest to smallest with the corresponding eigenmodes. The coefficients are calculated by multiplying the sorted eigenmodes by the transpose of the reorganized data matrix. This puts the eigenmodes and coefficients that captures the most information followed by the other eigenmodes and coefficients in decreasing order. Doing so allows the calculation of how many modes are needed to attain a certain amount of accuracy or data information, ie. 40 modes are needed in order to capture 95% of the data. This is accomplished by adding the normalized eigenvalues until the accuracy threshold is met.

IV. Results and Analysis

4.1 Median Analysis

The medians of the events for each latitude are in Figure 7. These graphs show the event day designated with a white line, latitudes are on the y-axis with the days numbered from the event day. The Vaisala network shows a clear band of dense lightning strikes as designated by the color bar around 13°N. The number of strikes after the event day is higher than before the event day. The lightning also increases across multiple latitudes after the event day. Conversely Earth Networks data shows a decrease in the number of strikes at approximately the same latitude. A second band at the equator also makes an appearance and shows a general increase in the number of strikes for that latitude. In both datasets the majority of the lightning does not exceed $\pm 50^{\circ}$ as most terrestrial storms are understood to develop between these latitudes. A clear northern latitudinal dependence can be seen in both datasets. This is due to more sensors being available in the northern hemispheres and because lightning frequency is higher over land than water. Note the scale difference of the colorbar between the two networks as Vaisala's colorbar maximum value is roughly three times larger than Earth Networks.

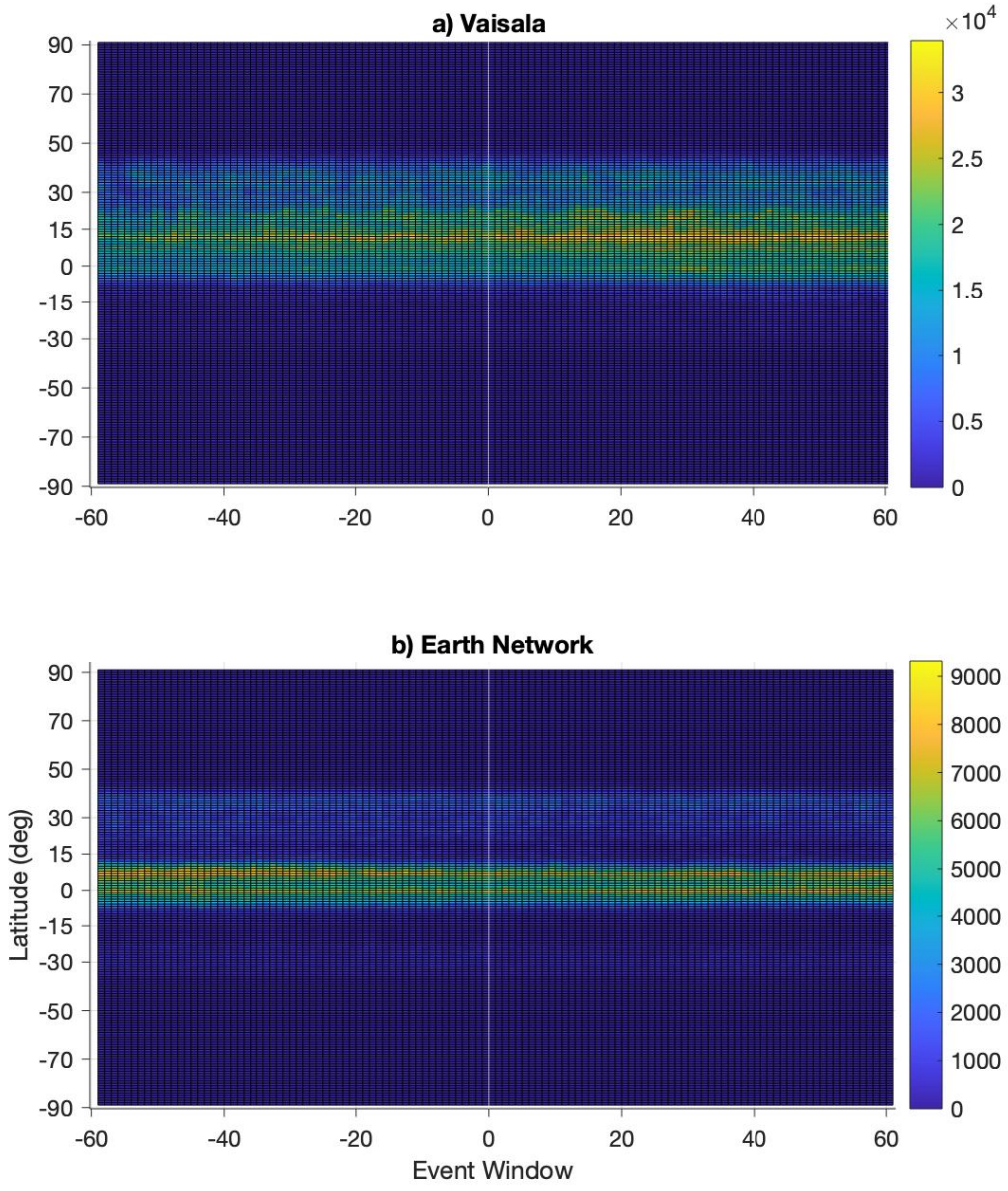

Figure 7: The median strikes per latitude by day over the event window with the trigger event day designated as a white line. Plot a shows the Vaisala Network's growth in lightning strikes especially around 13°N. The increase of lightning is not isolated to just one latitude but increases for surrounding latitudes. Plot b shows the variation in Earth Network's data. Two high count bands are pronounced around 0° and 11°N. The upper band shows a decrease in the lightning overall whereas the lower band appears to increase. Note the scale difference between the two networks. Vaisala's colorbar maximum is about roughly three times larger than Earth Networks.

A way to see more clearly if there is an increase or decrease in the median lightning is to use a ratio of the median of the lightning strikes of the days after the event over the median of the lightning strikes of the days prior. If the ratio is equal to 1 then the median lightning strikes for the 60 days after the event is the same as before. If the ratio is greater than 1 then there is an increase in the number of strikes, and vice versa for a ratio less than 1. Figure 8 show these ratios for each network. Not all latitudes had a defined ratio due to being equal to either 0 or infinity. Such results were not included in the graph.

The Vaisala data, shown in Figure 8, plot a, reveals an increase in the number of lightning strikes for all latitudes with less of an increase in the northern hemisphere than the southern. Conversely, Earth Networks' data does not behave the same. Two large dips around $\pm 18^{\circ}$ denote a decrease in the lighting occurrence. These particular latitudes roughly line up with the known Appleton anomaly that occurs $\pm 10^{\circ}$-15° of the magnetic equator [36]. The Appleton anomaly is caused by a fountain effect of uprising plasma [37]. The enhancement of the plasma density [37] at these latitudes may have a direct affect on lightning occurrence.

Figure 8 does not support the speculation that Earth's magnetic field line orientation would decrease lightning occurrence near the equator. Both Vaisala and Earth Network show an increase at the equator. An increase in lighting at high latitudes is only shown in the Vaisala data suggesting that the speculation that at higher latitudes Earth's magnetic field lines are more perpendicular to the surface allowing transport of more energetic particles into the lower atmosphere that may facilitate lightning onset is undetermined since Earth Network data does not support this.

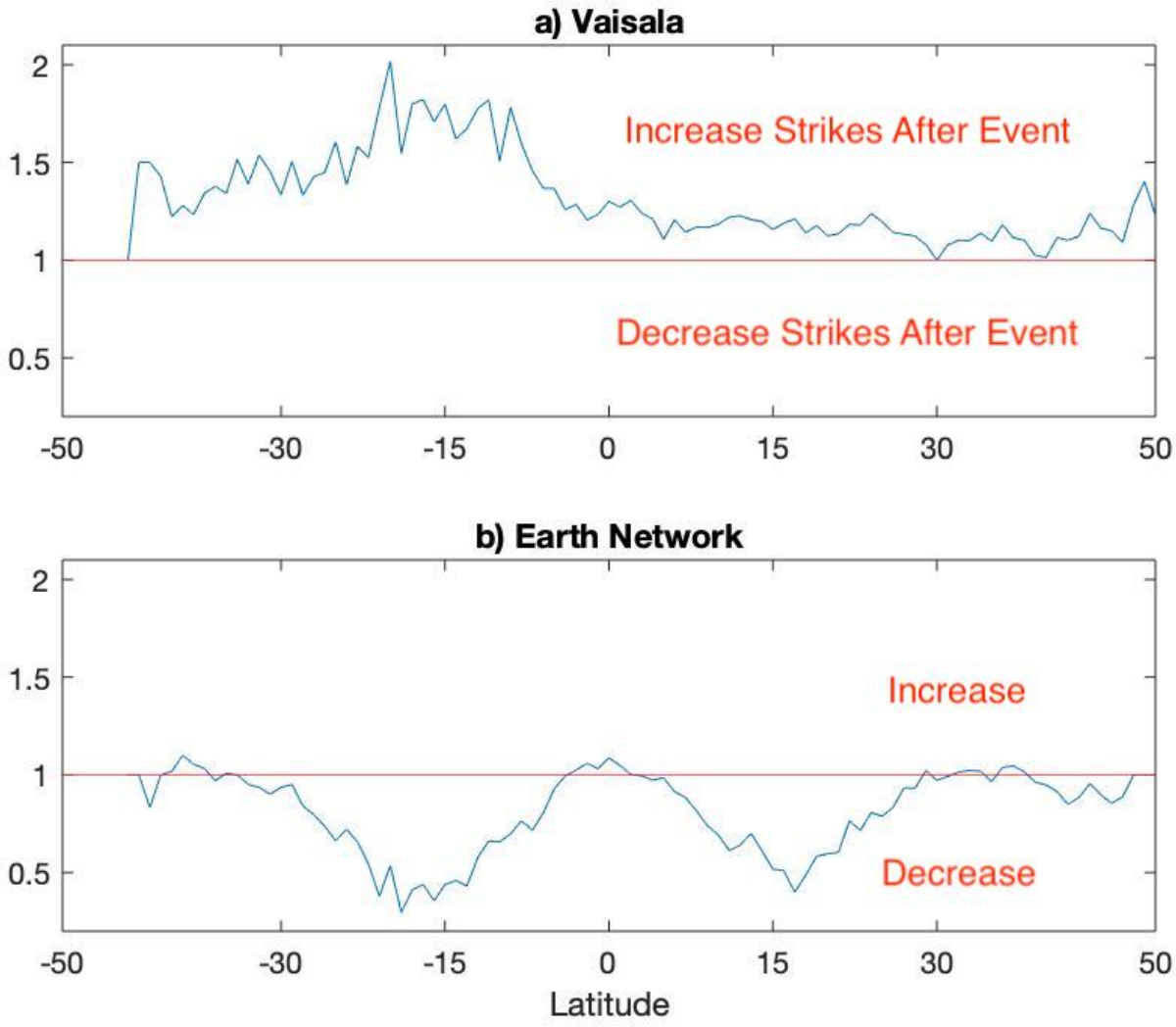

Figure 8: The ratio of the the median of the lightning strikes of the days after a trigger event over the median of the lightning strikes of the days prior. Plot (a) shows that the Vaisala data increases in lightning strikes for all latitudes for which the ratio is defined. Plot (b) shows Earth Networks' data is mostly decreasing but does have small sections of increasing strikes.

4.2 Fast Fourier Transform

An FFT was applied to both data sets in order to help ground the reader and for a comparison to the KLD method. Note that the DC term in the spectrum was removed by subtracting the mean, as is done in the KLD. Figure 9 shows that the low frequency modes are more important. The positive normalized mean of the squared values are shown for clarity. Both datasets give the same general shape with a difference in amplitudes.

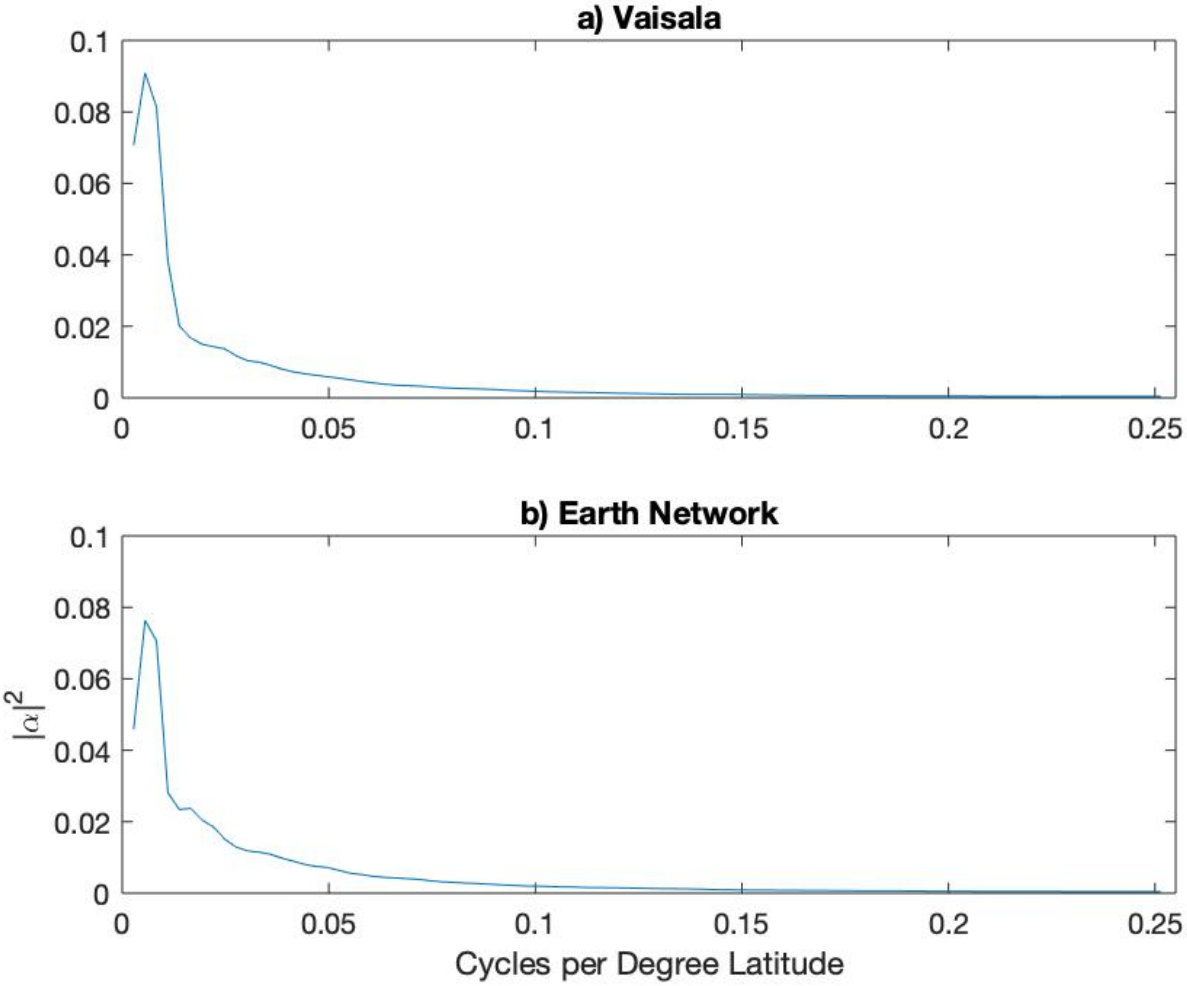

Figure 9: The positive half of the FFT power spectrum is graphed for the Vaisala and Earth Networks, parts (a) and (b) respectively, showing the importance of low frequency modes.

4.3 Karhunen-Loève Decomposition

4.3.1 KLD vs FFT

The eigenvalue spectrum and the required terms of the KLD and FFT are shown in Figures 10 and 11. For the KLD, eigenvalues are found when the covariance matrix K is diagonalized. For the FFT, comparable eigenvalues are calculated using Equation 4 using the magnitude of the Fourier coefficients as α. The eigenvalue spectra are organized from the highest value to lowest value, and the first 100 values are shown in the plots. The KLD eigenvalue spectrum amplitudes show that the values of the KLD capture more information than the FFT values, as shown in plots a and c. The general slope of the line indicates how quickly the method converges to the original data. Large terms capture more information early and the smaller terms capture the nuances of the data later. A steep line indicates that more data is captured with early terms and therefore convergences to the original data faster. There are many more terms required to reconstruct the smallest details of the data for the FFT than the KLD, as shown by the amplitude difference of 10^{-4} for the 100^{th} KLD eigenvalue vs 10^{-2} for the FFT 100^{th} eigenvalue. The number of terms required to reach 0.95, indicated by the red line, of the data is shown in plots b and d. The eigenvalues are normalized by $\frac{\lambda_i}{\sum_n \lambda_i}$, then added in order from largest to smallest until the cumulative sum is $\geq$0.95 [32]. The cumulative sum threshold is a measure of how much variation is needed to accurately reconstruct the data and the number of eigenvalues needed to reach the threshold describes how efficiently the expansion captures the data. It is shown that the FFT method requires many more terms than the KLD method. The Vaisala data KLD requires 40 terms vs 95 for the FFT to make the 95% threshold. Earth Networks data follows requiring 37 and 102 terms respectively. The entropy was verified to be lower for each network. The resulting values for the Earth Network data were 4.1 for the FFT expansion compared 2.9 for the KLD expansion. Vaisala

data had entropy values of 3.9 for the FFT expansion and 2.9 for the KLD expansion. For comparison, a random matrix of the same dimensions as the Vaisala data results in 5.1 for the KLD expansion.

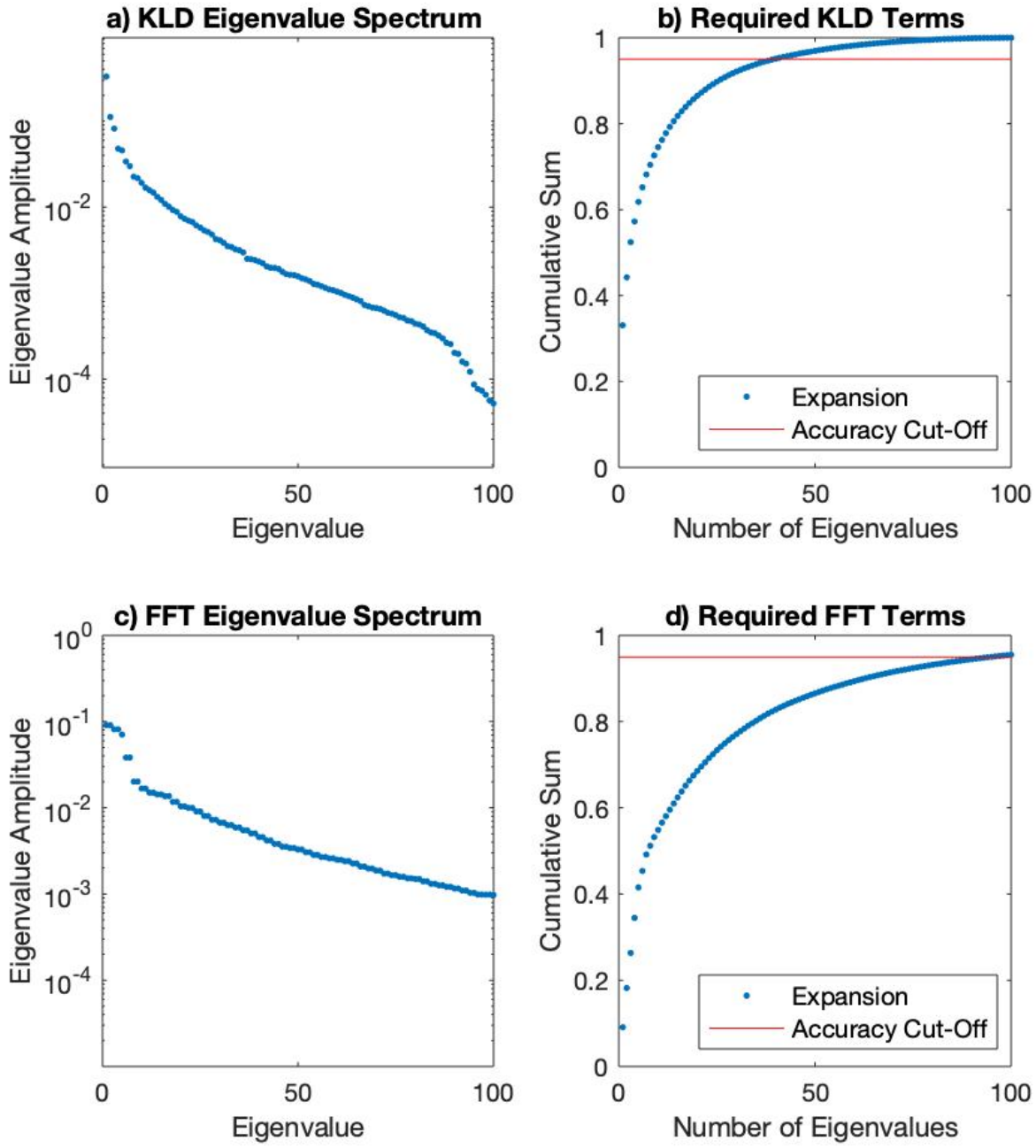

Figure 10: For the Vaisala data, plots a) and c) show the first 100 normalized eigenvalues ordered by magnitude for the KLD and FFT respectively. Plot a) has a steeper slope than plot c), indicating that the first few KLD modes are much larger than the first few FFT modes and capture more of the variation from the mean. In plots b) and d) the red line indicates the 0.95 cumulative sum threshold. Plots b) and d) show that the number of terms needed to attain the 0.95 threshold is lower for KLD than for the FFT, respectively. Entropy values are 3.9 and 2.9 for the FFT and KLD respectively.

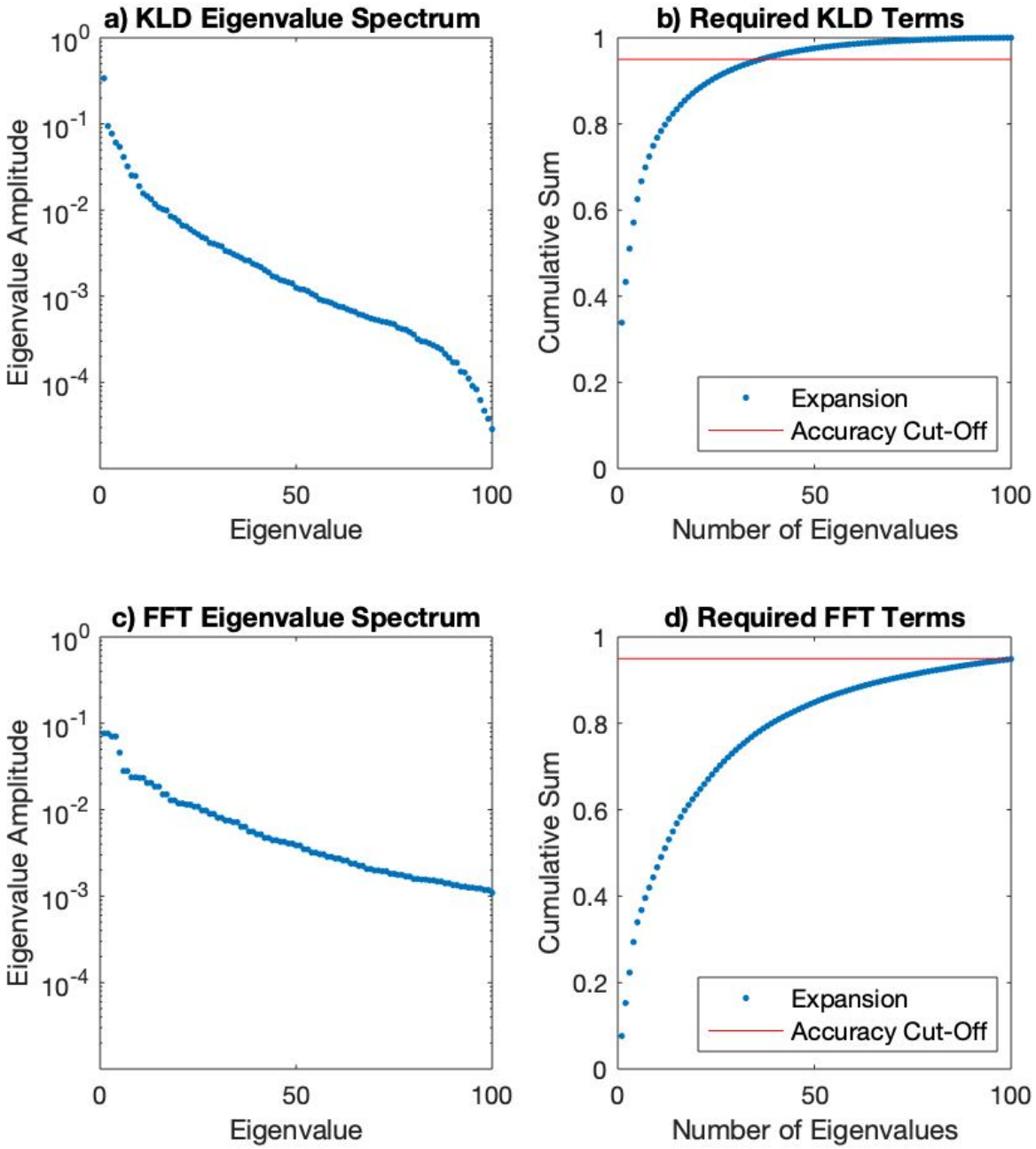

Figure 11: For the Earth Network data, plots a) and c) show the first 100 normalized eigenvalues ordered by magnitude for the KLD and FFT respectively. Plot a) has a steeper slope than plot c), indicating that the first few KLD modes are much larger than the first few FFT modes and capture more of the variation from the mean. In plots b) and d) the red line indicates the 0.95 cumulative sum threshold. Plots b) and d) show that the number of terms needed to attain the 0.95 threshold is lower for KLD than for the FFT, respectively. Entropy values are 4.1 and 2.8 for the FFT and KLD respectively.

4.3.2 KLD Modes

The mean of the strikes per latitude, Figure 12 below, shows a clear northern hemisphere dependence which supports the understanding that lightning occurs more often over land than sea. It is also consistent with the larger number of sensors in the northern hemisphere compared to the southern. The KLD method analyzes variations from these means.

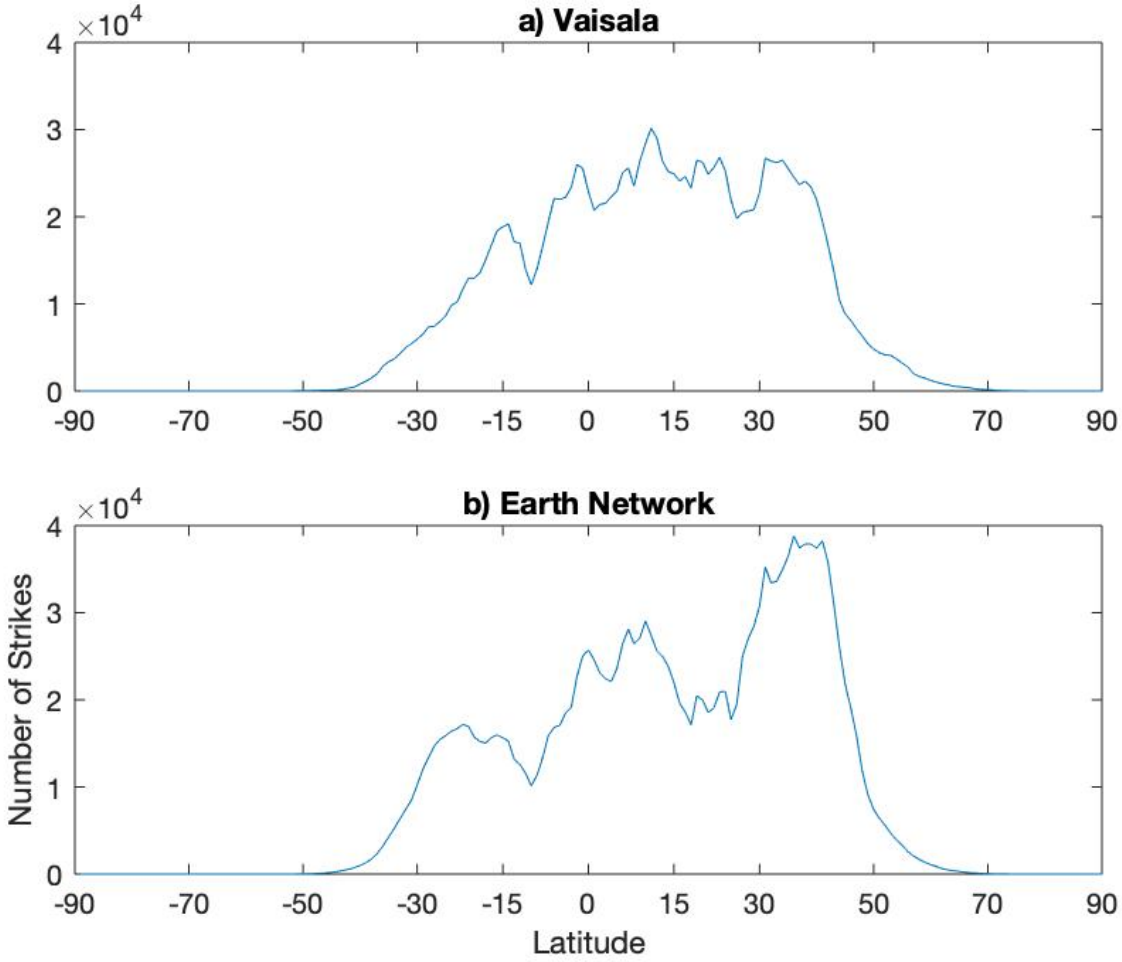

Figure 12: Mean strikes per latitude of the Vaisala (a) and Earth Network (b) datasets. A clear norther dependence is shown and supports that there is more lightning and detection sensors in the northern hemisphere. The KLD method analyzes variations off of these means.

The KLD method results in 181 modes and coefficients. The number comes from the spatial sampling of the data, which in this case is 181 degrees of latitude. The modes show by latitude where each matching coefficient either adds or subtracts strikes from the mean, Figure 12, depending upon positive/negative signs that come from the modes and coefficients. The first 25 modes are given in Figures 13 and 14 for the Vaisala and Earth Network data respectively. Early modes show long spatial frequencies that cover large swaths of latitudes. The later modes begin to capture the smaller variations and spikes in the data at higher latitudes, probably from more localized events.

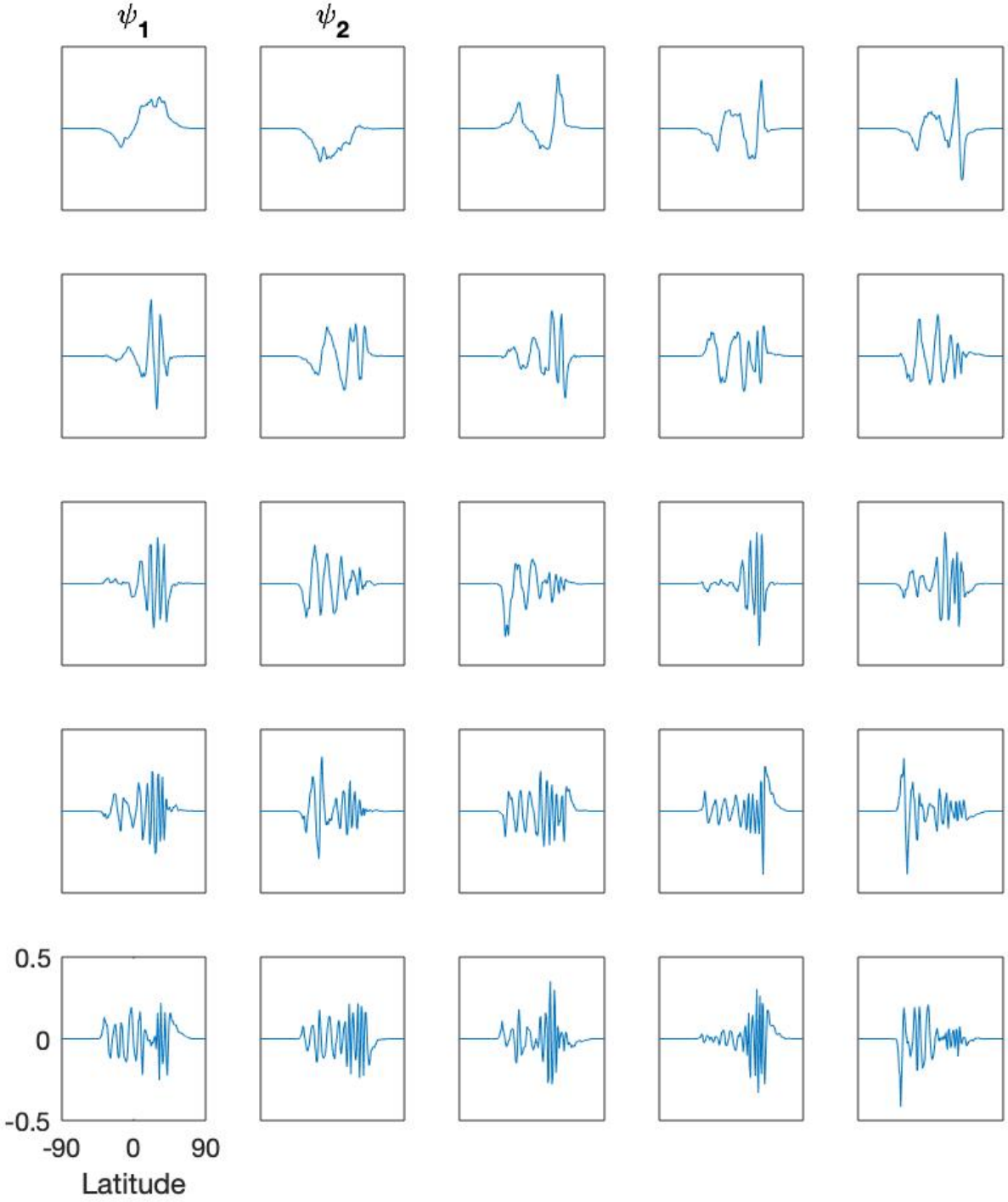

Figure 13: The early KLD modes for the Vaisala data exhibit a long spatial frequency that covers large swaths of latitude. Later modes capture smaller variances in the data and begin to capture lightning events at specific latitudes.

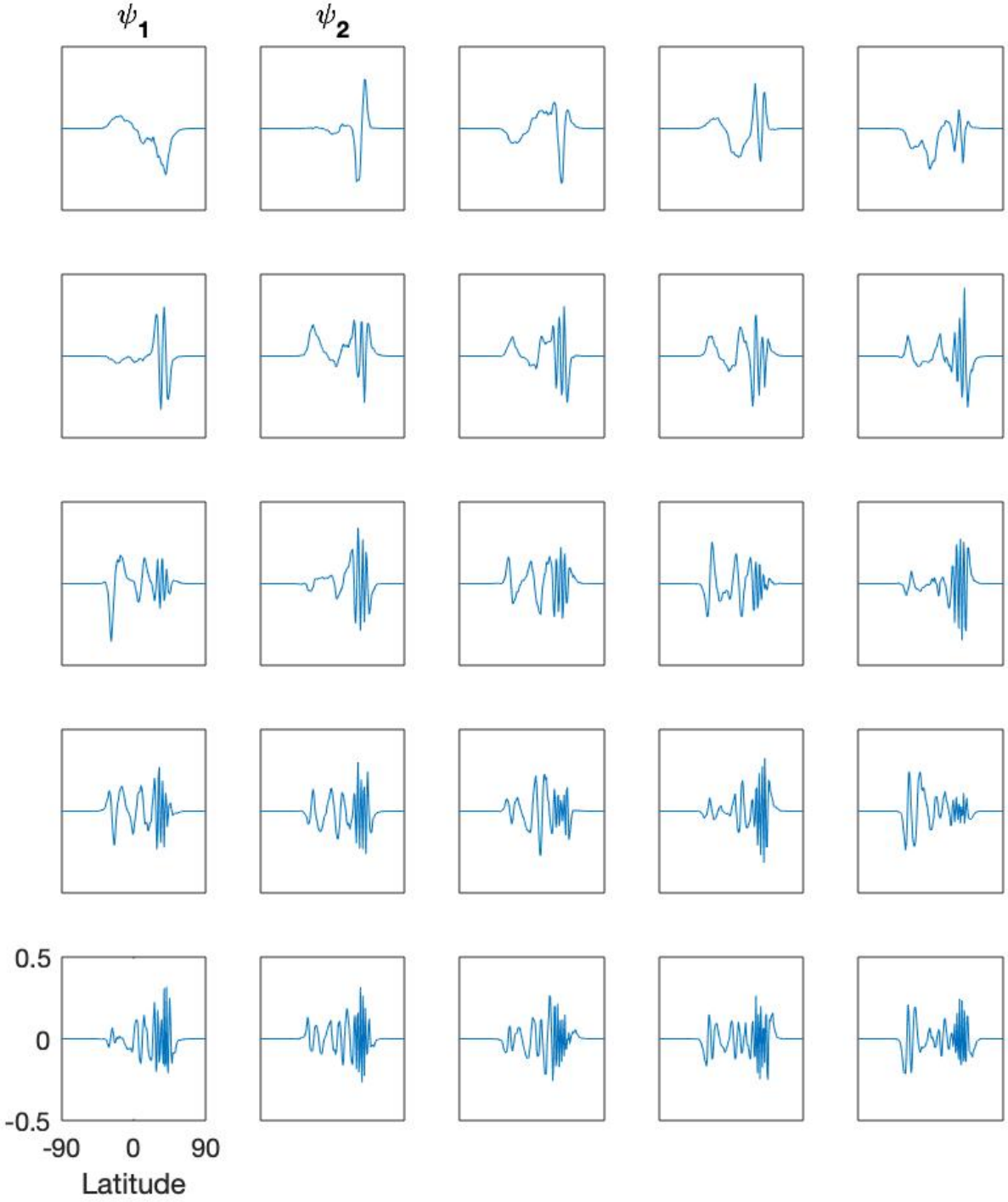

Figure 14: The early KLD modes for the Earth Network data exhibit a long spatial frequency that covers large swaths of latitude. Later modes capture smaller variances in the data and begin to capture lightning events at specific latitudes.

The modes generally follow the same pattern. The early modes do not have a lot of fluctuation and capture the overall condition of the information as compared to the later modes. The later modes capture more of the small details in the data as shown by the increase in fluctuations and the broadening further into the both hemispheres.

4.3.3 KLD Coefficients

The coefficients, $\alpha_i(t)$, of the KLD modes tells when the modes are significant. The large coefficients, when multiplied by a peak in the corresponding mode tells that there is more, or less depending on the sign, lightning strikes than the mean at that latitude. The first 25 coefficients are given in Figures 15 and 16 for the Vaisala and Earth Network data respectively.

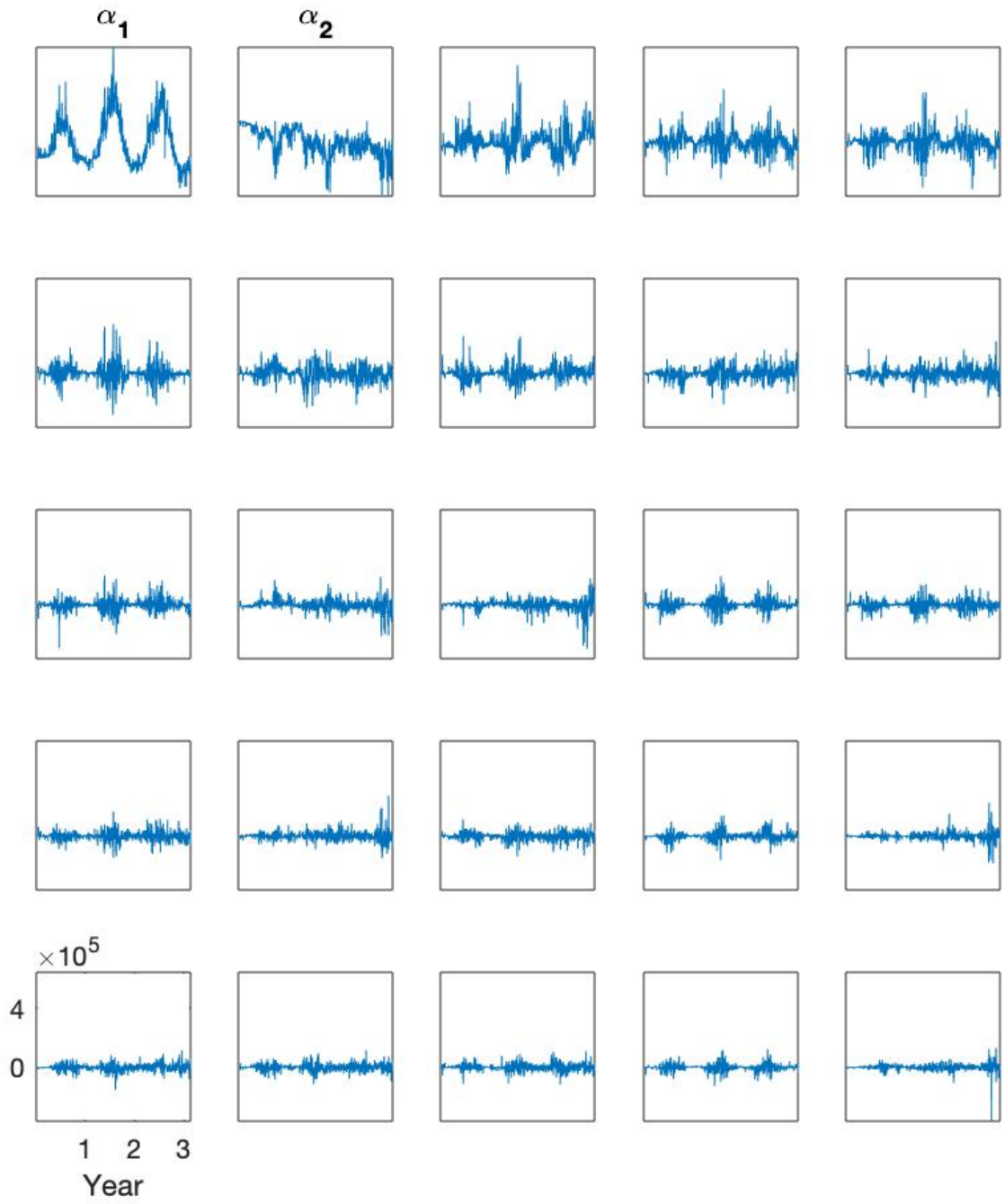

Figure 15: KLD coefficients for the Vaisala data. The seasonal variations can easily be seen in coefficients 1,6 and others. The amplitude of the coefficients determines how important the corresponding mode is at a particular time. The year indicates the length of time from the start of the data and does not correspond with the calendar year.

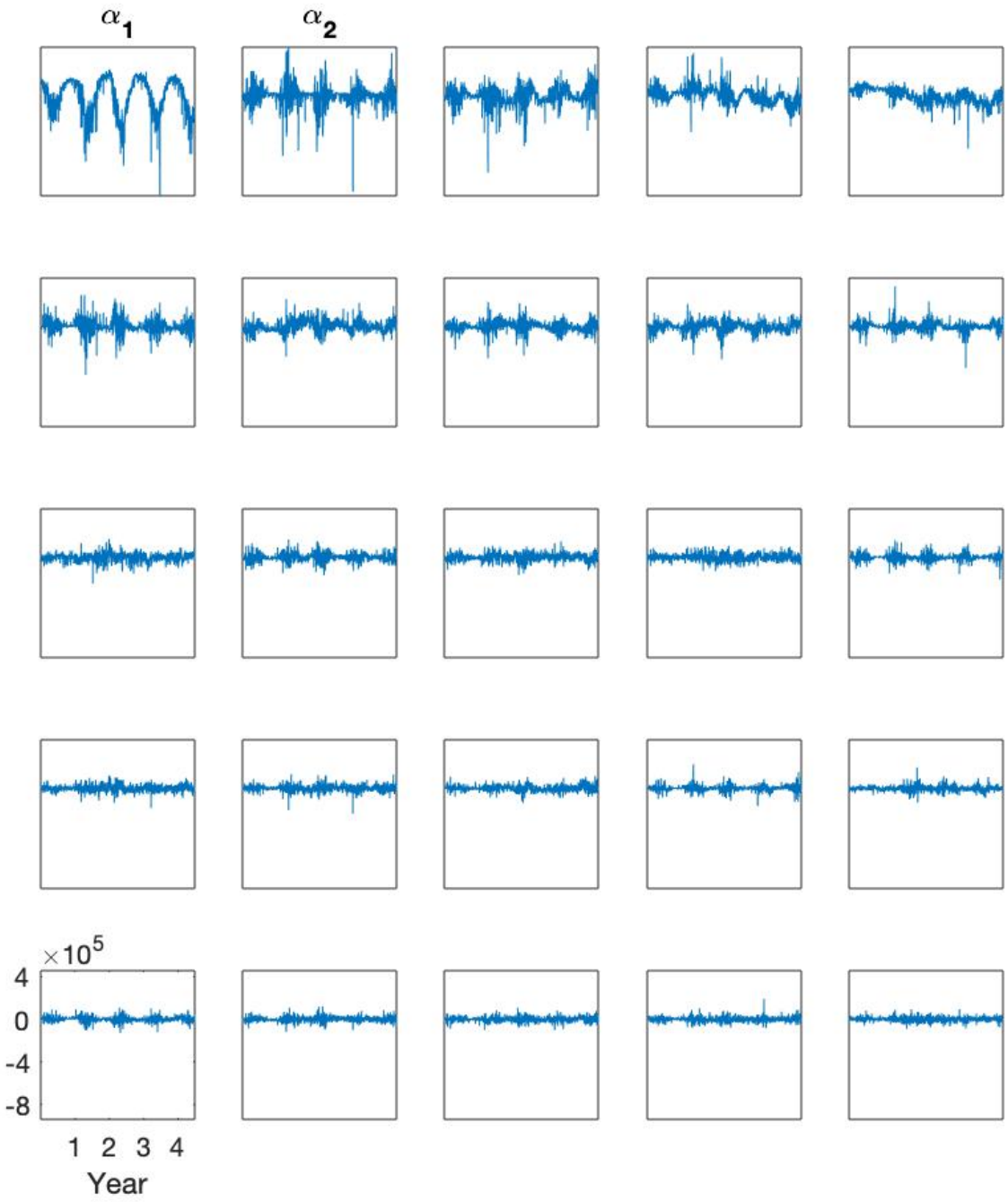

Figure 16: KLD coefficients of the Earth Network data. The seasonal variations can easily be seen in the first ten coefficients. The amplitude of the coefficients determines how important the corresponding mode is. The year indicates the length of time from the start of the data and does not correspond with the calendar year.

The first coefficient, and others, clearly show a seasonal dependence on the number of lightning strikes as seen by the wave or oscillatory behavior. Later coefficients in both data sets show similar behavior, but with much smaller amplitude which captures the smaller details of the data set. The first coefficients have a stark contrast in their shape but when multiplied by their respective modes, the product $\alpha_i(t)\psi_i(t)$ generates similar behavior which captures the dominating seasonal variation in lightning strikes. Figure 17 below helps visualize how $\alpha_1\psi_1 = [-\alpha_1][-\psi_1]$. When a peak value of α_1 (a) is multiplied by a value located in the northern hemisphere where ψ_1 (b) is positive, an increase in lightning is indicated by a positive product $\alpha_1\psi_1$. Similarly, if a downward peak from Earth Network α_1 (c) is multiplied by northern latitude where ψ_1 (d) is negative, $\alpha_1\psi_1$ results in a positive number resulting in an increase in lightning.

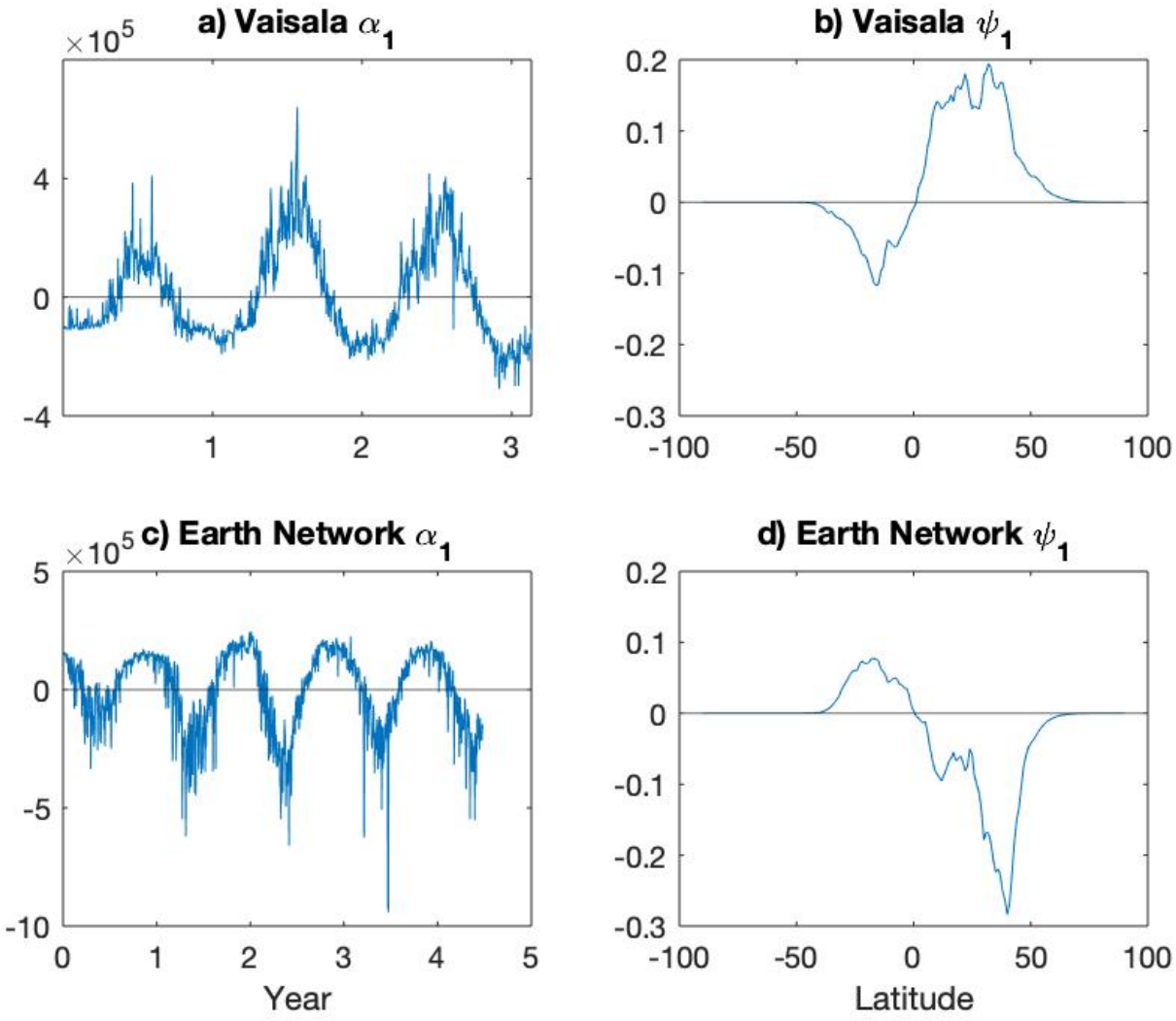

Figure 17: Coefficient α_1 and mode ψ_1 for Vaisala and Earth Network datasets (a), (b) and (c), (d) respectively. When a peak value of α_1 (a) is multiplied by a value located in the northern hemisphere where ψ_1 (b) is positive, an increase in lightning is indicated by a positive product $\alpha_1\psi_1$. Similarly, if a downward peak from Earth Network α_1 (c) is multiplied by northern latitude where ψ_1 (d) is negative, $\alpha_1\psi_1$ results in a positive number resulting in an increase in lightning. The KLD expansions capture the seasonal variation in both datasets.

Even though both datasets show similar characteristics, they have unique time-series shapes. For example, Vaisala's α_2 shows a decrease over time. This occurs for Earth Network at α_5, three coefficients later. When multiplying the respective coef-

ficients and modes together, both datasets result in similar lightning strike behavior. At the equator there is a decrease in lightning for the first 1.5-2 years and then an increase in later years. See Figure 18.

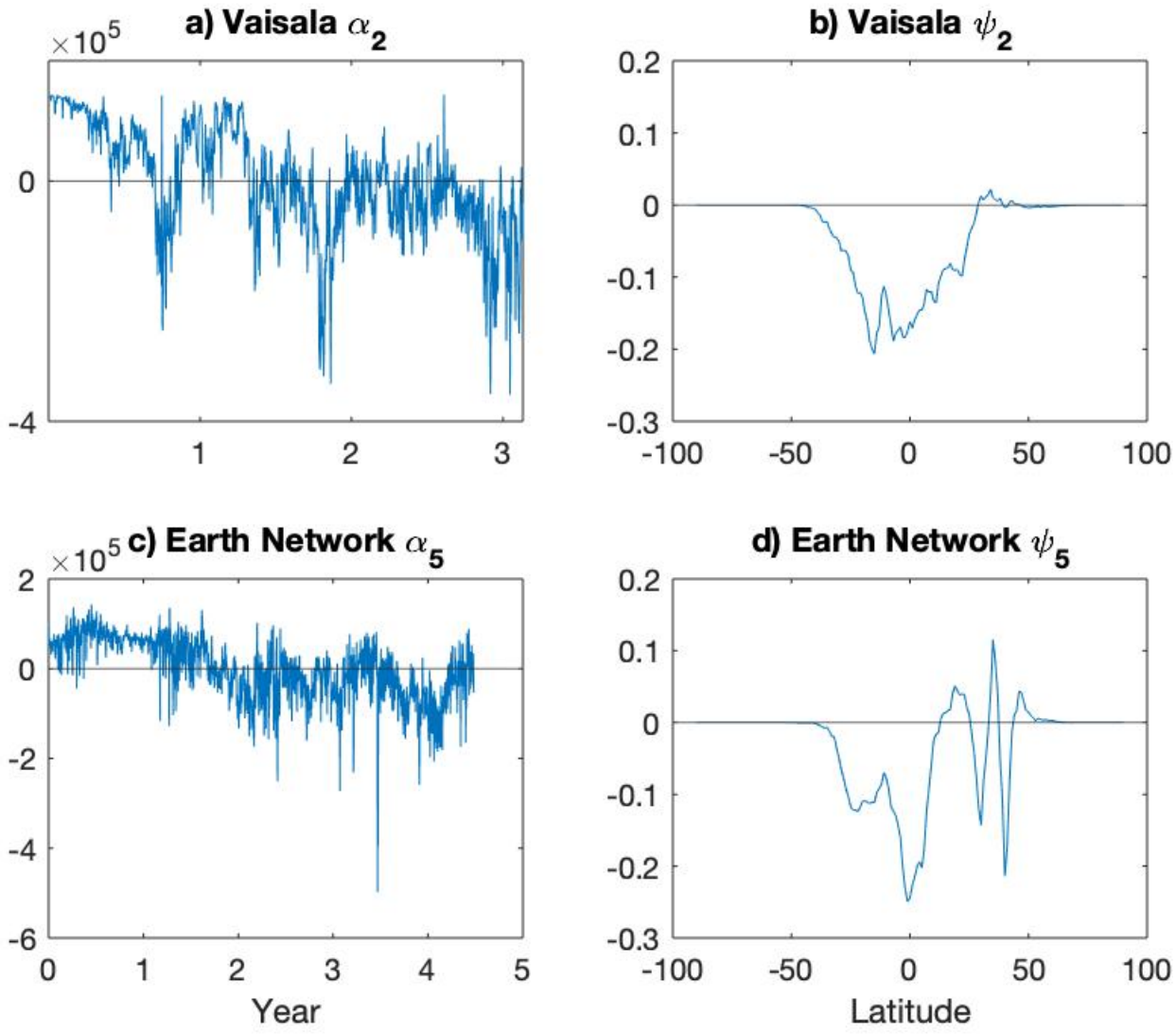

Figure 18: Coefficient α_2 and mode ψ_2 for Vaisala and α_5 and mode ψ_5 for Earth Network datasets (a), (b) and (c), (d) respectively. When an early value of α (a), (c) is multiplied by a value located at the equator where ψ (b), the product $\alpha\psi$ is negative resulting in less lightning than the mean at the equator. Similarly, a later value of α is multiplied by an equatorial ψ is negative and $\alpha\psi$ results in a positive number resulting in an increase in lightning. This is the same for both networks.

The KLD coefficients did not reveal any consistent solar cycle dependence. The combined sets of data span most of solar cycle 24 which began increasing in sun spot number approximately 2009 and has two peaks at years 2012 and 2014 with the later being the higher peak. Accordingly the Vaisala Network data set covers a significant amount of the growth time of cycle 24 while the Earth Network covers the highest peak and the majority of the decline of the cycle as seen in Figure 19. The coefficients do not appear to follow this trend with time. Further analysis of the all coefficients may yield results, though a visual analysis of Figures 15 and 16 containing only the first 25 coefficients is inconclusive.

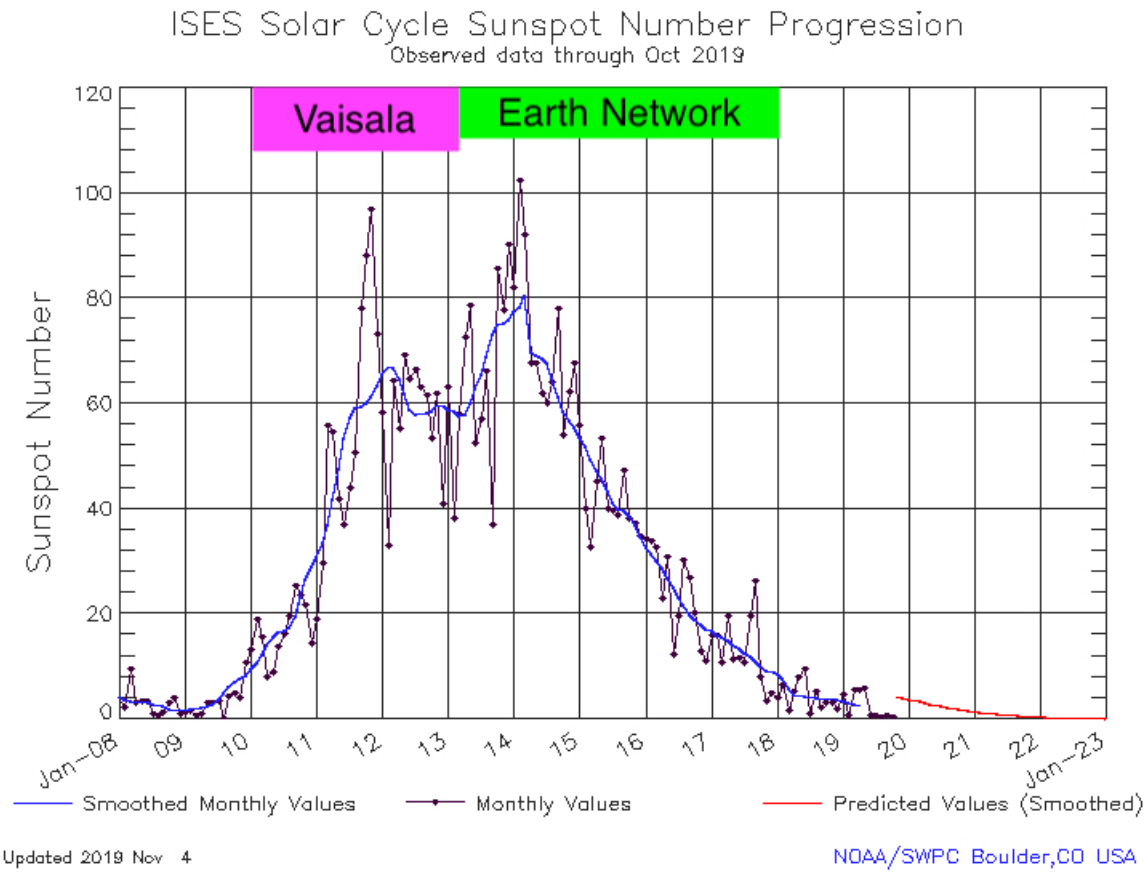

Figure 19: Solar Cycle 24 [38] by NOAA/SWPC showing the time frames during which the data of each network was recorded.

4.3.4 KLD Coefficients of the Event Windows

The median analysis method from section 3.2 was applied to the coefficients of each dataset. Each event window was applied to a coefficient and superimposed. The median was taken for each day to give a vector of a single coefficient over all the event windows. This was done for all coefficients with the results shown in Figures 20 and 21 for the Vaisala and Earth Network data respectively. The Vaisala data appears to have a general arch shape compared to the dipped shape that shows in the Earth Network data.

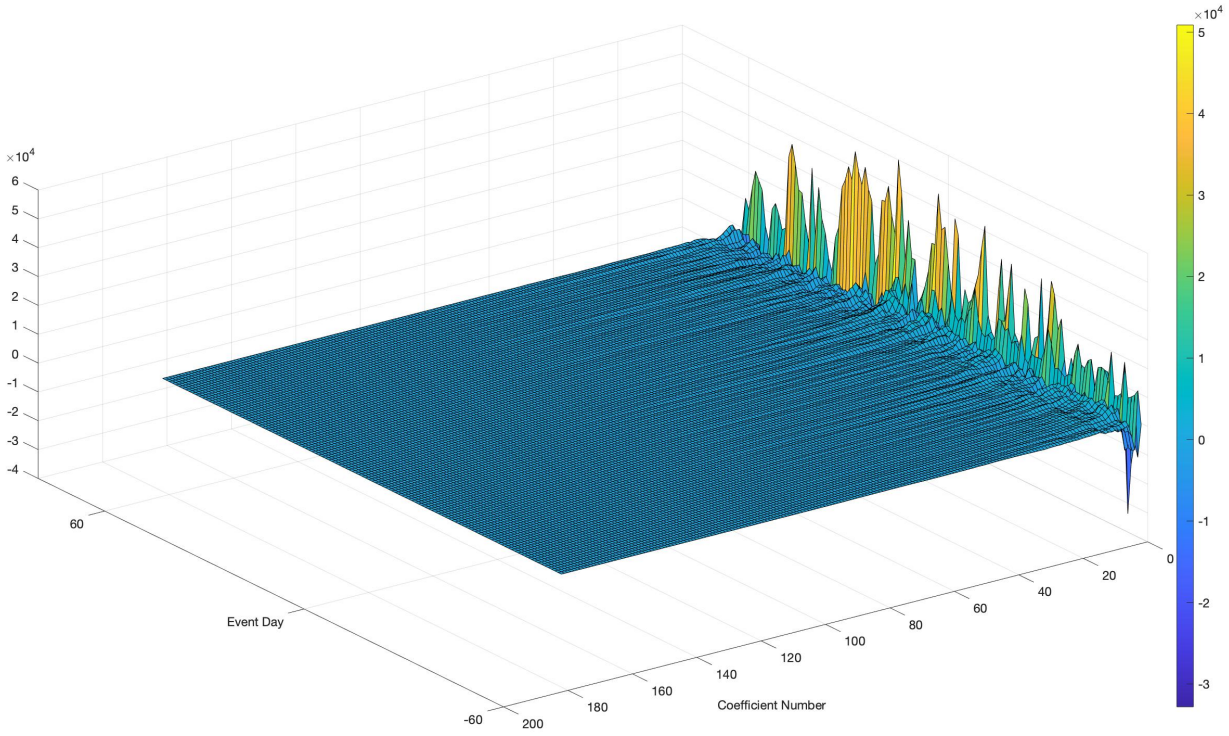

Figure 20: Showing the median of all the KLD coefficients of the Vaisala data over all the event windows. The beginning coefficients located in the back capture the majority of the variance of the data. Later coefficients have little impact on capturing the information of the events. The general shape of first coefficients is an arch. This is distinctly different than the Earth Network data in Figure 21.

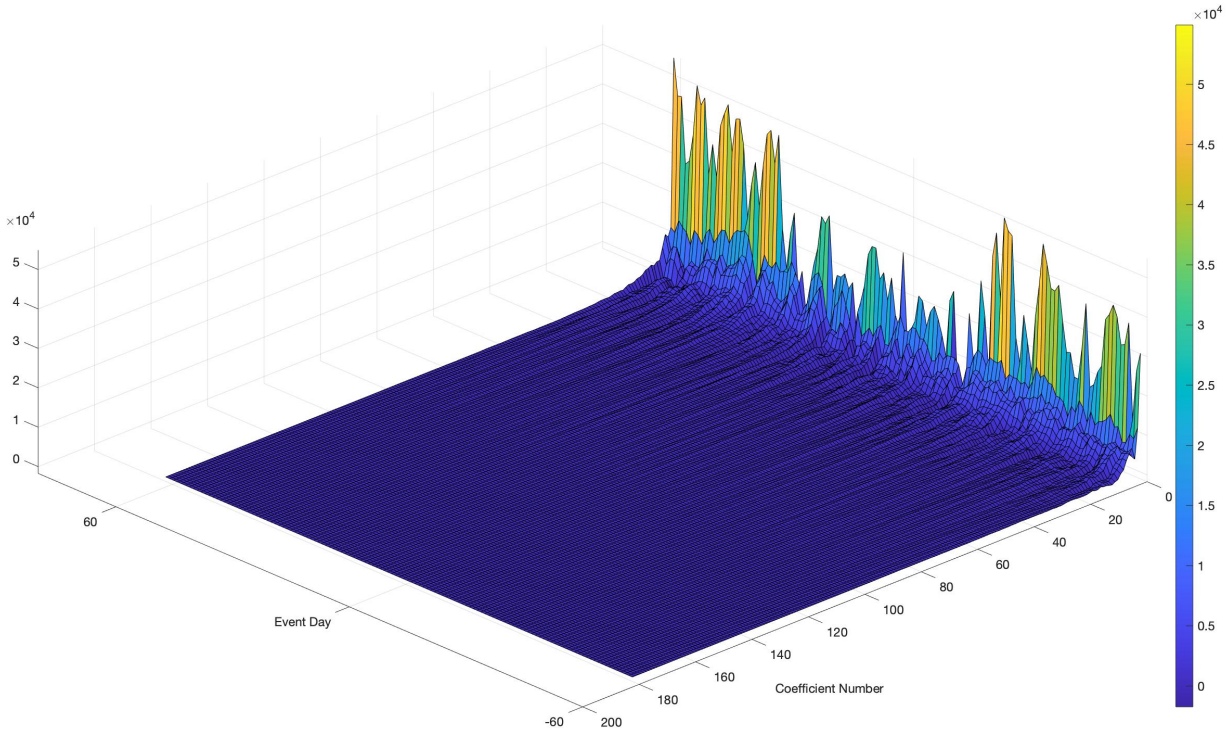

Figure 21: Showing the median of all the KLD coefficients of the Earth Network data over all the event windows. The beginning coefficients located in the back capture the majority of the variance of the data. Later coefficients have little impact on capturing the information of the events. The general shape of the first coefficients has a dip in the middle around the event day. This is distinctly different than the Vaisala data in Figure 20.

Comparing the first six event window coefficients reveals differences between the two datasets. Figure 22 shows the Vaisala and Earth Network coefficients in plots a and b respectively. The event window coefficient α_1 for both networks dominates in amplitude though the shapes are vastly different due to the KLD method. The Vaisala α_1 amplitude increases as time approaches the event day and then decreases after. Conversely the Earth Network decreases toward the event day and then increases. The later days after the event in the Vaisala data appears to do more offsetting to the α_1 compared to Earth Network where the amplitudes of the first six coefficients

are positive.

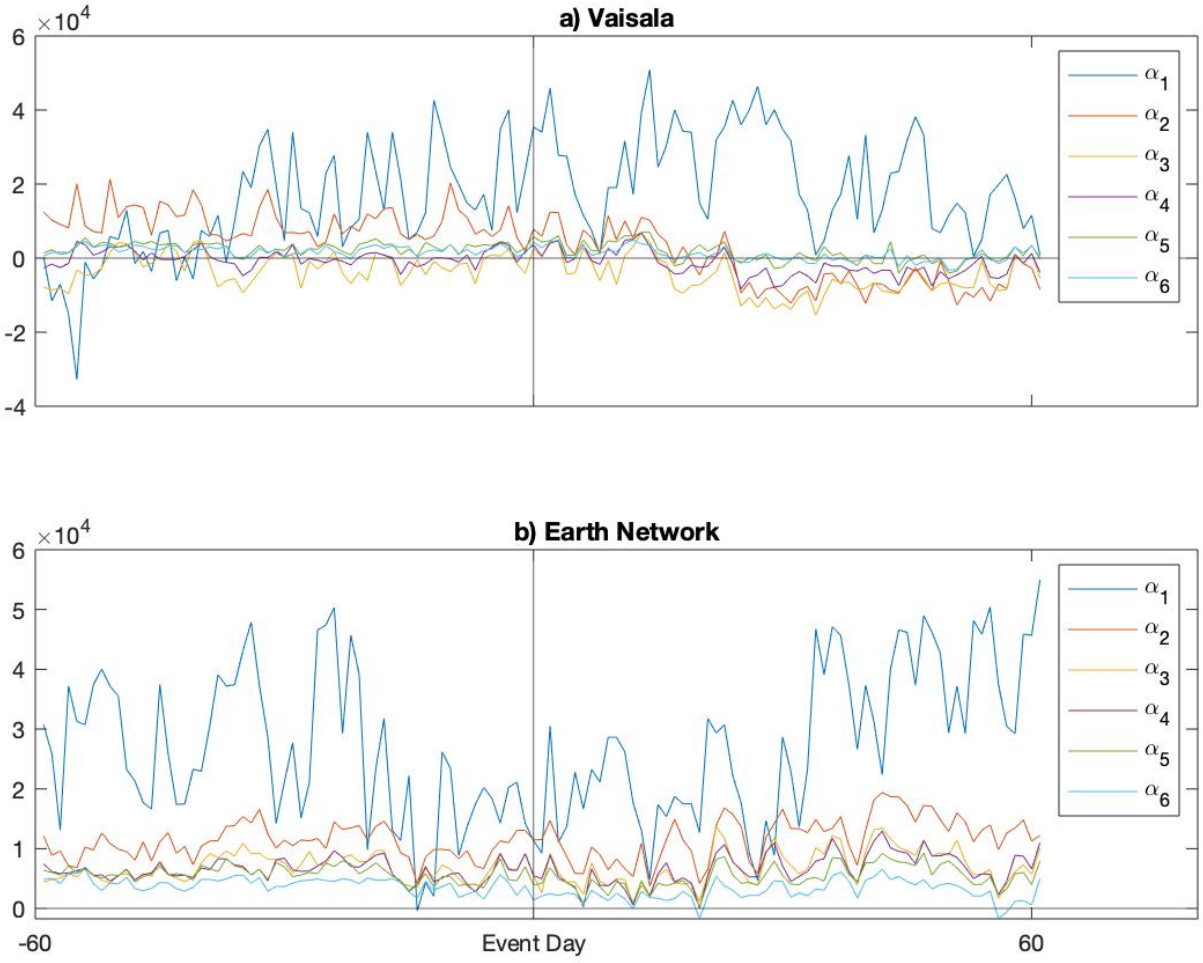

Figure 22: Medians of the coefficients over the events for the first six α_i's for the Vaisala (a) and Earth Network (b). Coefficient α_1 dominates in both but has different shapes. Other coefficient medians from Vaisala have a decrease after the event day compared to almost no change in the Earth Network.

The first event window coefficients for both networks are the dominating feature in Figure 22. The KLD method resulted in opposite shapes. Recall that in Figure 17, mode ψ_1 for Vaisala appears to be an inverse-like of Earth Network ψ_1. Taking the Earth Network event window coefficient α_1 and multiplying it by -1 to match the Vaisala event window coefficient, Figure 22, and mode ψ_1, Figure 17, results in

Figure 23. Both networks show a decrease in the coefficient amplitude after an event. Earth Network shows a more sudden decrease around 35 days after the event. The mode ψ_n gives the variation by latitude. Latitudes will have an increase or decrease in lightning depending if $\psi < 0$ or $\psi > 0$ as determined by $\alpha_n \psi_n$. Note that the shape of the graph would be opposite if the Vaisala event window coefficient is multiplied by -1 instead of the Earth Network event window coefficient but the product $\alpha_n \psi_n$ still gives the same increase or decrease in lightning at latitudes. The similar behavior implies that both networks and their respective KLD capture the same phenomenon after a solar wind event. The amplitude difference is because of the difference in the number of strikes between the two networks.

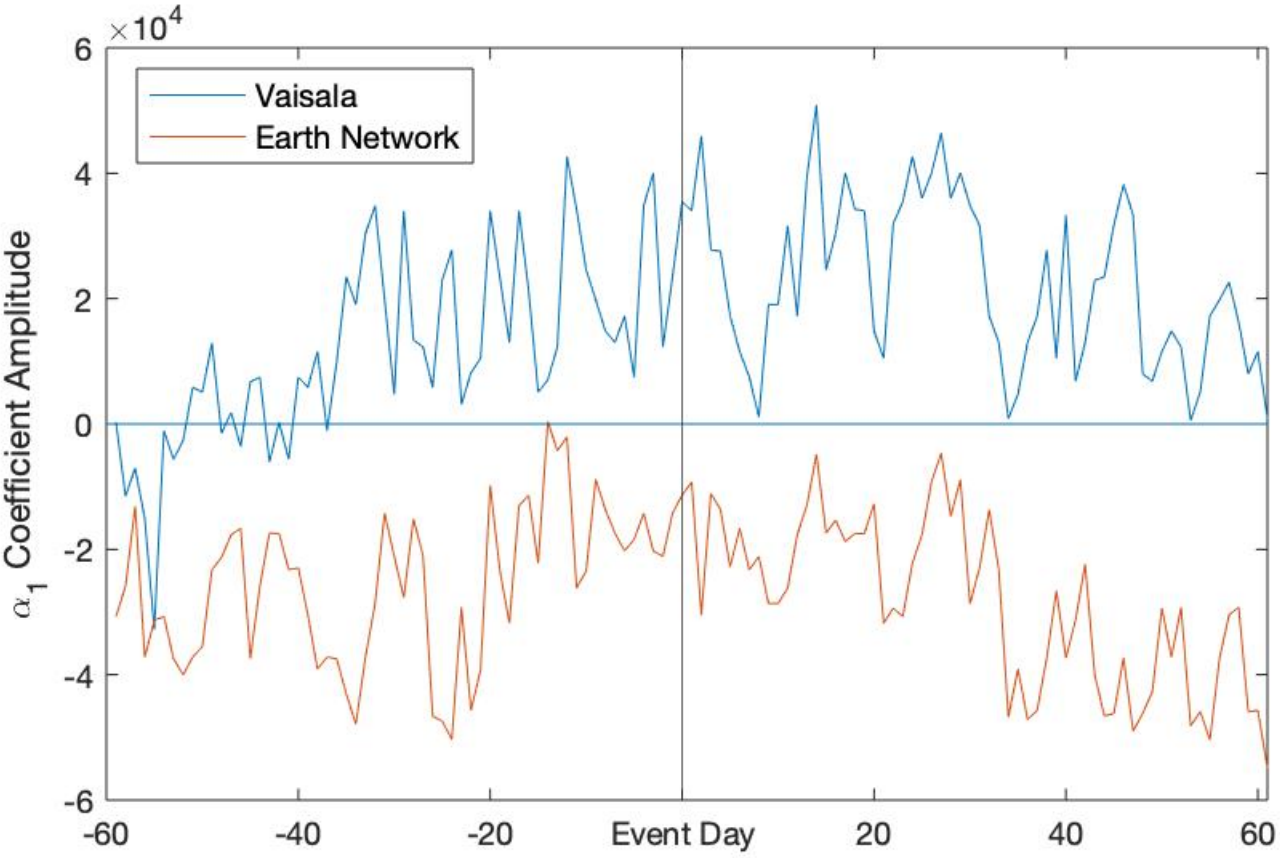

Figure 23: The median of α_1 over all events for Earth Network is multiplied by -1. This results in very similar shape to Vaisala's event window coefficient α_1. Both networks show a decrease in the coefficient amplitude after an event as well as similar lightning increase or decrease depending on latitude determined by $\alpha_i \psi_i$. The difference in amplitude is due to the differences in the number of strikes between the two datasets.

General trends appear to form after the first few coefficients as illustrated in Figure 24. These trends do not directly offset the large amplitude on α_1 but seem to continue the small ripples as seen in coefficients ranging from 20-40 in Figure 20. This illustrates that the early coefficients capture most of the data and the rest of the coefficients are for the smaller variations and modulations of the early coefficients.

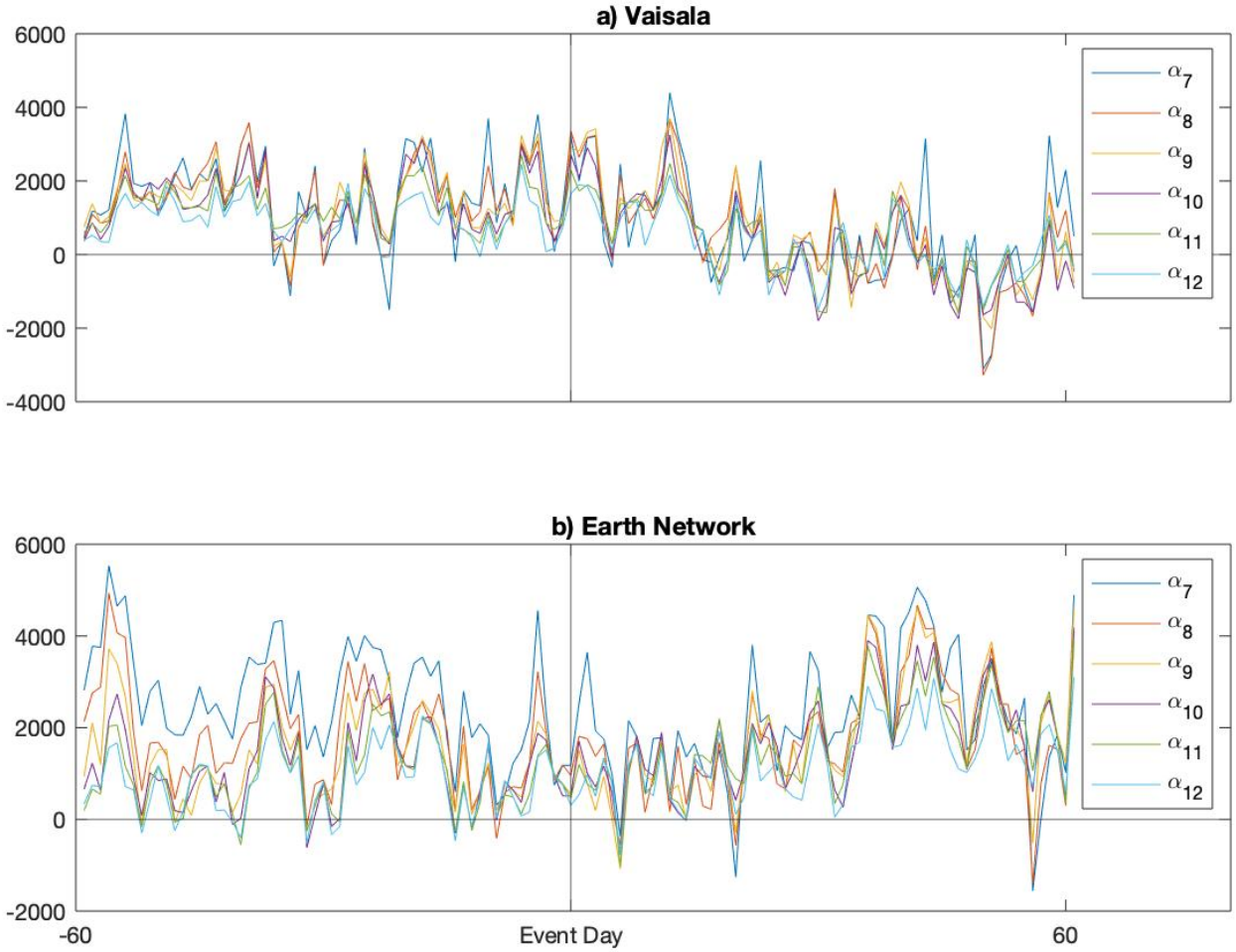

Figure 24: Medians of the coefficients over the events for α_6 to α_{12} for the Vaisala (a) and Earth Network (b). The medians in both networks follow the same shape of the respective network. Vaisala shows a general decrease after the event day. Earth Network reveals a general increase and less variance between the coefficient medians than before the event day.

V. Conclusions

The total velocity of the solar wind was used in determining solar wind events defined as an increase of 75 km/s or more in five hours [1]. No seasonal distribution of solar wind speed events is evident which implies that seasonal lightning variation is not dependent upon solar wind events. Seasonal lightning distribution is therefore caused by a possible combination of network sensor locations and land area.

The lightning data was split into two datasets after comparing a duplicate day. It was found that the Earth Network data counted 266,971 more strikes than the Vaisala Network for the same latitudes and longitudes.

Datasets from the Vaisala and Earth Network lightning detection networks were analyzed using a median method similar to Scott et al [1]. Event windows are defined as ± 60 days of the solar wind event [1]. The ratio of median of lighting strikes of the days after an event over the days prior to the event by latitude was graphed. The Vaisala data shows an increase over all latitudes of lightning strikes when the solar wind speed increases, particularly in the southern hemisphere. Earth Network data shows a general decrease in strikes, especially around the $\pm 15^{\circ}$ latitudes which may be caused by the Appleton anomaly [36]. Both show an increase in lighting around the equator and at high latitudes of around 30° to 50°. The speculation of the Earth's magnetic field orientation affecting lightning initiation due to solar wind events does not hold in this study. The speculation leads to a decrease in lightning occurrence over the equator. This study found a consistent increase in lighting over the equator in both networks using the median analysis method.

Entropy comparisons were made between the FFT and KLD methods resulting in a lower entropy for KLD method than the FFT for both networks. The resulting values for the Earth Network data were 4.1 for the FFT expansion compared 2.9 for the KLD expansion. Vaisala data had entropy values of 3.9 for the FFT expansion

and 2.9 for the KLD expansion. The lower entropy supports that the KLD method captures information with fewer modes. The Vaisala data KLD requires 40 terms vs 95 for the FFT to make the 95% threshold. Earth Networks data follows similarly requiring 37 and 102 terms, respectively.

The KLD method was applied to the datasets to create modes and coefficients that capture the data in the most efficient way possible as variations from the mean. Early modes and coefficients capture the large variations of the data and later modes and coefficients capture the smaller details of the data. The seasonal variation is clearly shown in the KLD methodology for both networks in the dominant first coefficient but a solar cycle dependence is not seen in the coefficients. Both networks show the same increase or decrease in lightning activity by latitude of the first coefficient and mode as denoted by the variation from the mean $\alpha_1(t)\psi_1(t)$.

The first 12 coefficients of were analyzed by event window for each network. Both networks show the same increase or decrease in lightning activity by latitude after a solar wind event when looking at the first event window coefficient. The KLD event window method captures the same lightning phenomenon for both networks.

A direct comparison of the Scott et al [1] paper cannot be concluded. Scott et al [1] used the UK Met Office's ATD network for lightning strike counts which is not the data source for this study. Scott et al [1] also used the v_y component of the solar wind velocity as the trigger source. This study used the overall velocity speed as the trigger source. It may be that the v_y component is important to the correlation. Instances occurred in which a second trigger day was included in the event window. Excluding timelines during which no other trigger events occurred would change the results and may reveal different behaviors.

The median analysis shows that the two networks do not behave the same way, which could be due to the different data collection methods. Conversely, the KLD

method shows the networks behave similarly from analysis of the first, second and fifth coefficients and modes. The KLD event window method supports similar behavior.

The median analysis by latitude gave different results for the Vaisala and Earth Network datasets. The KLD pulled out some common features such as the seasonal dependence and a general increase in lightning at the equator. Comparisons between different datasets must be handled carefully. The KLD method may be a way to capture common features, or assess how similar the datasets are.

5.1 Future Work

Further analysis of the differences and impacts in the Vaisala and Earth Network data collection methodology should be considered for future studies. The v_y component of the solar wind velocity should be compared to the global lightning data sets to verify Scott et al findings. Other solar parameters could be analyzed in a similar method presented in this paper to find other correlations in areas such as magnetic field components. A study similar to this one using the same time frames as well as lighting data from a satellite such as Tropical Rainfall Measuring Mission (TRMM) sensor would further illuminate which network is able to capture the most information. A comparison of individual coefficients from each network would also help determine if the networks are capturing similar data beyond the first event window coefficient. A similar study based on geomagnetic latitudes would also help understand correlations between the magnetic characteristics of the solar wind and Earth's magnetic field in relation to terrestrial weather.

Bibliography

1. C. Scott, R. Harrison, M. Owens, M. Lockwood, and L. Barnard, "Evidence for solar wind modulation of lightning," *Environmental Research Letters*, vol. 9, no. 5, p. 055004, 2014.

2. O. P. Neto, I. R. Pinto, and O. Pinto Jr, "The relationship between thunderstorm and solar activity for brazil from 1951 to 2009," *Journal of Atmospheric and Solar-Terrestrial Physics*, vol. 98, pp. 12–21, 2013.

3. A. A. Petrukovich, M. M. Mogilevsky, A. A. Chernyshov, and D. R. Shklyar, "Some aspects of magnetosphere–ionosphere relations," *Physics-Uspekhi*, vol. 58, no. 6, p. 606, 2015.

4. M. J. Rycroft, "Thunder and lightning—what determines where and when thunderstorms occur?" *Environmental Research Letters*, vol. 9, no. 12, p. 121001, 2014.

5. Ace real time solar wind. [Online]. Available: https://www.swpc.noaa.gov/products/ace-real-time-solar-wind,LastcheckedMar2020

6. Dscovr space weather data portal. [Online]. Available: https://www.ngdc.noaa.gov/dscovr/portal/index.html#/,LastcheckedMar2020

7. R. Roussel-Dupré, J. Colman, E. Symbalisty, D. Sentman, and V. P. Pasko, "Physical processes related to discharges in planetary atmospheres," in *Planetary Atmospheric Electricity*. Springer, 2008, pp. 51–82.

8. Noaa's first operational satellite in deep space reaches final orbit. [Online]. Available: https://www.nasa.gov/feature/goddard/nation-s-first-operational-satellite-in-deep-space-reaches-final-orbit,LastcheckedMar2020

9. Severe weather 101, lightning basics. [Online]. Available: https://www.nssl.noaa.gov/education/svrwx101/lightning/,LastcheckedMar2020

10. D. M. Le Vine. (1987) Review of measurements of the rf spectrum of radiation from lightning. [Online]. Available: https://ntrs.nasa.gov/archive/nasa/casi.ntrs.nasa.gov/19870001225.pdf,LastcheckedMar2020

11. Chapter 6 - electromagnetic methods of lightning detection. [Online]. Available: https://library.wmo.int/doc_num.php?explnum_id=3184,LastcheckedMar2020

12. R. L. Dowden, J. B. Brundell, and C. J. Rodger, "Vlf lightning location by time of group arrival (toga) at multiple sites," *Journal of Atmospheric and Solar-Terrestrial Physics*, vol. 64, no. 7, pp. 817–830, 2002.

13. S. D. Rudlosky and D. T. Shea, "Evaluating wwlln performance relative to trmm/lis," *Geophysical Research Letters*, vol. 40, no. 10, pp. 2344–2348, 2013.

14. Lightning detection networks. [Online]. Available: https://www.vaisala.com/en/products/systems/lightning-detection-networks,LastcheckedFeb2020

15. S. D. Rudlosky, M. J. Peterson, and D. T. Kahn, "Gld360 performance relative to trmm lis," *Journal of Atmospheric and Oceanic Technology*, vol. 34, no. 6, pp. 1307–1322, 2017.

16. R. Said, U. Inan, and K. Cummins, "Long-range lightning geolocation using a vlf radio atmospheric waveform bank," *Journal of Geophysical Research: Atmospheres*, vol. 115, no. D23, 2010.

17. R. Said, M. Cohen, and U. Inan, "Highly intense lightning over the oceans: Estimated peak currents from global gld360 observations," *Journal of Geophysical Research: Atmospheres*, vol. 118, no. 13, pp. 6905–6915, 2013.

18. B. Lustig. Earth networks advances lightning detection capabilities, press release. [Online]. Available: https://www.earthnetworks.com/blog/earth-networks-advances-lightning-detection-capabilities-expanded-global-network/,LastcheckedFeb2020

19. E. Networks, "Personal correspondence," Email, Jan 2020.

20. S. Heckman, "Entln status update," in *XV International Conference on Atmospheric Electricity*, 2014, pp. 15–20.

21. C. Liu and S. Heckman, "Total lightning data and real-time severe storm prediction," in *TECO-2012: WMO Tech. Conf. on Meteorological and Environmental Instruments and Methods of Observation*, 2012.

22. C. Rodger, S. Werner, J. Brundell, E. Lay, N. Thomson, R. Holzworth, and R. Dowden, "Detection efficiency of the vlf world-wide lightning location network (wwlln): initial case study," 2006.

23. S. D. Rudlosky, "Evaluating ground-based lightning detection networks using trmm/lis observations," in *23rd International Lightning Detection Conference & 5th International Lightning Meteorology Conference*, 2014.

24. J. Manninen, T. Turunen, N. Kleimenova, M. Rycroft, L. Gromova, and I. Sirviö, "Unusually high frequency natural vlf radio emissions observed during daytime in northern finland," *Environmental Research Letters*, vol. 11, no. 12, p. 124006, 2016.

25. M. Shwehdi, "Thunderstorm distribution and frequency in saudi arabia," *Journal of Geophysics and Engineering*, vol. 2, no. 3, pp. 252–267, 2005.

26. S. Desch, W. Borucki, C. Russell, and A. Bar-Nun, "Progress in planetary lightning," *Reports on Progress in Physics*, vol. 65, no. 6, p. 955, 2002.

27. M. Owens, C. Scott, M. Lockwood, L. Barnard, R. Harrison, K. Nicoll, C. Watt, and A. Bennett, "Modulation of uk lightning by heliospheric magnetic field polarity," *Environmental Research Letters*, vol. 9, no. 11, p. 115009, 2014.

28. M. Kirby, *Geometric data analysis: an empirical approach to dimensionality reduction and the study of patterns*. John Wiley & Sons, Inc., 2000.

29. M. D. Graham and I. G. Kevrekidis, "Alternative approaches to the karhunen-loeve decomposition for model reduction and data analysis," *Computers & chemical engineering*, vol. 20, no. 5, pp. 495–506, 1996.

30. P. J. Holmes, J. L. Lumley, G. Berkooz, J. C. Mattingly, and R. W. Wittenberg, "Low-dimensional models of coherent structures in turbulence," *Physics Reports*, vol. 287, no. 4, pp. 337–384, 1997.

31. A. Szumski, "Finding the interference–the karhunen–loève transform as an instrument to detect weak rf signals," *Inside GNSS*, vol. 6, no. 3, pp. 56–64, 2011.

32. A. L. Franz, R. Roy, L. B. Shaw, and I. B. Schwartz, "Effect of multiple time delays on intensity fluctuation dynamics in fiber ring lasers," *Physical Review E*, vol. 78, no. 1, p. 016208, 2008.

33. S. M. Zoldi and H. S. Greenside, "Karhunen-loeve decomposition of extensive chaos," *Physical review letters*, vol. 78, no. 9, p. 1687, 1997.

34. I. Triandaf and I. B. Schwartz, "Karhunen-loeve mode control of chaos in a reaction-diffusion process," *Physical Review E*, vol. 56, no. 1, p. 204, 1997.

35. S. Watanabe, "Karhunen-loeve expansion and factor analysis: theoretical remarks and application," in *Trans. on 4th Prague Conf. Information Theory, Statistic Decision Functions, and Random Processes Prague*, 1965, pp. 635–660.

36. H. Lühr, M. Rother, S. Maus, W. Mai, and D. Cooke, "The diamagnetic effect of the equatorial appleton anomaly: Its characteristics and impact on geomagnetic field modeling," *Geophysical Research Letters*, vol. 30, no. 17, 2003.

37. Ionospheric currents. [Online]. Available: https://geomag.colorado.edu/ionospheric-currents.html,LastcheckedFeb2020

38. Solar cycle 24. [Online]. Available: https://en.wikipedia.org/wiki/Solar_cycle_24, LastcheckedMar2020

REPORT DOCUMENTATION PAGE

Form Approved
OMB No. 0704–0188

1. REPORT DATE *(DD–MM–YYYY)*	2. REPORT TYPE	3. DATES COVERED *(From — To)*
26–03–2020	Master's Thesis	Sept 2018 — Mar 2020

4. TITLE AND SUBTITLE

Modulation of Lightning Occurrence by the Solar Wind

5a. CONTRACT NUMBER

5b. GRANT NUMBER

5c. PROGRAM ELEMENT NUMBER

6. AUTHOR(S)

Capt Adam L. Baxter

5d. PROJECT NUMBER

5e. TASK NUMBER

5f. WORK UNIT NUMBER

7. PERFORMING ORGANIZATION NAME(S) AND ADDRESS(ES)

Air Force Institute of Technology
Graduate School of Engineering and Management (AFIT/EN)
2950 Hobson Way
WPAFB OH 45433-7765

8. PERFORMING ORGANIZATION REPORT NUMBER

AFIT-ENP-MS-20-M-079

9. SPONSORING / MONITORING AGENCY NAME(S) AND ADDRESS(ES)

AFOSR/RTB
875 N Randolph St Suite 3000 Arlington VA 22203
DSN 426-9586, COMM 703-696-9586
Email: julie.moses@us.af.mil

10. SPONSOR/MONITOR'S ACRONYM(S)

AFOSR/RTB

11. SPONSOR/MONITOR'S REPORT NUMBER(S)

12. DISTRIBUTION / AVAILABILITY STATEMENT

DISTRIBUTION STATEMENT A:
APPROVED FOR PUBLIC RELEASE; DISTRIBUTION UNLIMITED.

13. SUPPLEMENTARY NOTES

14. ABSTRACT

Lightning affects military and civilian operations. Characterization of the distribution of global lightning strikes of two detection networks based on solar wind events is analyzed. the median analysis by latitude gave different results for the two network datasets. The KLD pulled out some common features such as the seasonal dependence and a general increase in lightning at the equator. Comparisons between different datasets must be handled carefully. the KLD method may be a way to capture common features, or assess how similar the datasets are. A detailed analysis of the differences between the tow networks detection algorithms and investigating other space weather parameters should be accomplished in the future.

15. SUBJECT TERMS

Global Lightning Strikes, Solar Wind, Space Weather, Terrestrial Weather

16. SECURITY CLASSIFICATION OF:			17. LIMITATION OF ABSTRACT	18. NUMBER OF PAGES	19a. NAME OF RESPONSIBLE PERSON
a. REPORT	b. ABSTRACT	c. THIS PAGE			Captain Adam L. Baxter, AFIT/ENP
U	U	U	UU	61	19b. TELEPHONE NUMBER *(include area code)* adam.baxter@afit.edu